FATIGUE DAMAGE ASSESSMENT OF FACE CENTRED CUBIC (FCC) METALS & ALLOYS

BY

OSEI OWUSU-KORKOR

B.Sc., Dip. Ed., UCC (1992)

A THESIS PRESENTED TO THE DEPARTMENT OF PHYSICS

UNIVERSITY OF CAPE COAST, CAPE COAST

IN PARTIAL FULFILMENT OF THE REQUIREMENT

FOR THE AWARD OF MASTER OF PHILOSOPHY DEGREE IN PHYSICS

MAY, 1997

TABLE OF CONTENTS

DECLARATION

I declare that the work reported in this thesis is the result of my own research activities except where otherwise specified in the text, and that it has not been submitted previously to this or any other University for any degree.

..... 8/7/97

OSEI OWUSU-KORKOR

(BSc. (Physics), Dip. Ed)

.....

Prof. A. AYENSU

(PRINCIPAL SUPERVISOR)

.....

DR. K.A. DANSO

(CO-SUPERVISOR)

.....

Mr. G. K. QUAINOO 8/7/97

(CO-SUPERVISOR)

DEDICATION

This thesis is dedicated to: My father, Mr. Osei Hwidieh; my brother, Kwaku Owusu Akyempim and my beloved wife, Rita Osei Owusu.

ACKNOWLEDGEMENTS

I am very grateful to Prof. Akwasi Ayensu (my main supervisor) for his counsel and guidance which has taken me through this project. My sincere gratitude also goes to my co-supervisors Dr. K.A Danso and Mr.G.K. Quainoo, and the technical staff at Non-destuctive Testing Section and Physics Department of Ghana Atomic Energy Commission (Kwabenya) for their suggestions and assistance given during the research.

I am also grateful to Prof. A.N. de-Heer Amissah (former Head of Department) for provision of research facilities. My thanks are also due to the lecturers in the Physics Department (UCC) for their encouragement during the period that the project was underway. I wish to express my thanks and appreciation to Mr.L.A. Ahen and the Technical staff of Physics Department for providing the much needed support services and guidance.

I am also grateful to Mr.W.N.A. Hammond of Science Workshop (UCC) and his staff, especially Messrs S Brown and J.A. Fynn for assisting with the fabrication of the test specimens. I also wish to express my gratitude and appreciation to Mr.J. Amarteifio for introducing me to darkroom techniques of processing optical micrographs. I also wish to thank Dr.A.B.C. Dadson (UST), Mr A.O. Nunoo of UST Physics Department, and to Messrs K. Essilfie and Agyei Boateng, both of Mechanical Engineering Department (UST) for introducing me to the fatigue testing machine and impact testing equipment, in addition to providing technical assistance.

Finally, I wish to thank Miss Gertrude Quansah and Miss Mavis Amponsah Larbi for helping with the typing.

SYNOPSIS

Cyclic fatigue tests were conducted at low and high temperatures on annealed and polished samples of polycrystalline Copper, Alpha-brass, Aluminium, Mild steel (0.25 %C) and Stainless steel (18Cr-8Ni) with grain sizes of 341.2 μm, 150.0 μm, 72.5 μm, 63.5 μm and 45.0 μm respectively. Prior to fatigue test, non-destructive testing (NDT) was performed to check for the presence of any surface and internal flaws. To obtain data on ductility and strength of the specimens, impacts tests were performed to evaluate the different materials and set up limits of stresses to be applied.

The endurance limit, σ_e, obtained from the Wohler S-n curves at room temperature for Cu, Cu-30%Zn, Al, Mild steel and Stainless steel samples were 62.9 MPa, 97.0 MPa, 173.3 MPa, 228.1 MPa and 303.5 MPa respectively. It was observed that the fatigue strength of the materials show a decrease with temperature increase. Optical micrographs of deformed specimens revealed the formation of cavities and coalescence of micro-cracks into macro-cracks.

For the interpretation of the experimental results, the model for damage based on Paris law,

$$\frac{da}{dn} = C(\Delta K)^m$$

was analysed, where da/dN is the crack growth rate (i.e. per cycle), m is the crack growth rate exponent, ΔK is stress intensity C is the crack growth rate coefficient. The fatigue damage assessment show that: (i) fatigue limit is directly related to the inverse half-power of grain size; (ii) over the range 10^{-7}-10^{-2} mm/Cycle, the Paris law produces stable crack growth for stainless steel and aluminium; (iii) fatigue deformation results from residual stresses which cause crack opening and propagation and (iv) the specimens failed by cup and cone fracture.

LIST OF FIGURES

LIST OF TABLES

LIST OF SYMBOLS

a	Crack length (m)
C	Crack growth rate coefficient
C_o	Elber"s constant for crack growth rate coefficient
D	Specimen diameter (m)
d	Grain size (μm)
E_N	Fracture energy of notched specimen (J)
E_u	Fracture energy of un-notched specimen (J)
f	The number of dislocation pile-up in the length g between a source within the grain and grain boundary
K_{max}	Maximum applied stress (MPa)
K_{min}	Minimum applied stress (MPa)
K_{open}	Applied stress intensity
L	Length between gauge diameter and threaded end of specimen (m)
$\bar{L}$	Mean linear intercept grain size(μm)
l_c	Critical crack length (m)
m	Crack growth rate exponent
n	Number of cycles to failure (Hz)
T	Temperature (K)
W	Total applied load (N)
W_1	Weight of load pan (N)
W_2	Applied load (N)
UTS	Ultimate tensile strength (MPa)
Z	Section modulus of specimen

ΔK	Cyclic stress intensity (MPa)
ΔK_{eff}	Effective stress intensity (MPa)
δ	Length between a source within the grain and grain boundary (m)
η	Total number of readings
σ	Applied stress (MPa)
$\bar{\sigma}$	Mean stress (MPa)
σ_e	Endurance limit (MPa)
σ_{max}	Maximum stress (MPa)
σ_{min}	Minimum stress (MPa)

CHAPTER ONE

INTRODUCTION

1.1. Fatigue Phenomena

Fatigue of materials refers to the changes in properties (that leads to fracture) as a result of cyclic loads. Research into the deformation and fracture of materials by fatigue dates back to the nineteenth century. However, along with the development of "science of materials" and "fracture mechanics" in recent decade, fatigue of materials has also emerged as a major area of scientific and applied research which encompasses such diverse disciplines as materials science (including science of metals, ceramics, polymers and composites), mechanical, civil and aerospace engineering, biomechanics, applied Physics and applied mathematics. With the increasing emphasis on advanced materials, the scope of fatigue research continues to broaden at a rapid pace.

A descriptive definition of fatigue is found in the report entitled General Principles for Fatigue Testing of metals [1], where fatigue is defined as "changes in properties which can occur in a metallic material due to the repeated application of stresses or strains". Although the term fatigue applies specially to those changes which lead to cracking or failure of metals, the description is also generally valid for the fatigue of non metallic materials.

Fatigue occurs in many different forms. Fluctuations in externally applied stresses or strains only result in mechanical fatigue. Cyclic loads acting in association with high temperatures cause creep-fatigue, when the temperature of the cyclically loaded component also fluctuates, thermomechanical fatigue (i.e. a combination of thermal and mechanical fatigue) is induced. Recurring loads imposed in the presence of a chemically aggressive or embrittling environment give rise to corrosion-fatigue. The repeated application of load in conjunction with rolling contact between materials produces rolling contact fatigue, while fretting fatigue occurs as a result

of pulsating stresses along with oscillatory relative motion and frictional sliding between surfaces. Fatigue failures generally take place under the influence of cyclic loads where peak values are considerably smaller than the "safe" loads estimated on the basis of static fracture analyses.

Wohler [2] conducted systematic investigation of fatigue fracture in rail road axles for the German Railway Industry. He observed that the strength of steel axles subjected to cyclic loads was appreciably lower than the static strength. His work also led to the characterization of fatigue behaviour in terms of stress amplitude-life (S-n) curves and to the concept of fatigue "endurance limit".

Interpretations of fatigue mechanisms based on microscopic flaws and optical micrographs of cyclic damage on the specimen surface by Ewing and Humfrey [3] showed convincingly that slip bands developed in many grains of the polycrystalline material. Those slip bands broadened with the progression of fatigue deformation and led to the formation of cracks; catastrophic failure of the specimen was investigated by the growth of single dominant flaw.

The notion that plastic strains are responsible for cyclic damage was established thro-ugh the Coffin-Manson relationship [4, 5], following the classic work of Inglis [6] and Griffith [7]. The mathematical tool for quantitative treatments of fatigue fracture was developed by Irwin [8] who showed that the amplitude of the stress singularity ahead of a crack could be expressed in terms of the scalar quantity known as the stress intensity factor ΔK. Paris, Gormez and Anderson [9] suggested that the increment of fatigue crack advance per stress cycle, da/dn could be related to the range of stress intensity factor, ΔK, during constant amplitude cyclic loading.

Although fatigue failure under fixed amplitudes of cyclic stresses generally forms the basis for fundamental studies, service conditions in engineering applications invariably involve the exposure of structural components to variable amplitude spectrum loads, corrosive environments, low or elevated temperatures and multi axial stress states. The development of reliable life

prediction models which are capable of handling such complex service conditions in one of the toughest challenges in fatigue research. Suresh [10] has discussed fatigue life prediction models and these will be reviewed in sections 1.2 to 1.5.

1.2. Micromechanism Approach to Fatigue

The different stages of fatigue damage in engineering component are whereby defects may nucleate in an initially undamaged section and propagate in stable manner until catastrophic fracture ensues. The progression of fatigue damage can be broadly classified into the following stages: (a) substructural and microstructural changes which cause nucleation of permanent damage, creation of microscopic cracks, growth and coalescence of microscopic flaws to form"dominant" cracks, (stage of fatigue generally constitutes the demarcation between crack initiation and propagation), (b) The formation of the dominant crack generally constitutes stable propagation of the dominant micro crack, structural instability, complete fracture or catastrophic failure.

A major obstacle to the development of life prediction models for fatigue lies in the choice of a definition for crack initiation. Materials scientists concerned with the microscopic mechanisms of fatigue are likely to regard the nucleation of a micrometer size flaw (~1 μm^2) along slip bands and grain boundaries [11], and the roughening of fatigue surfaces as the crack inception stage of fatigue failure.

A practicing engineer, on the other hand, tends to relate the limit of resolution of the (non-destructive) crack detection equipment (typically a function of a millimetre ~ 1 μm) with the nucleation of a fatigue crack and with the initial crack size used for design.

1.3. Total-life Approach to Fatigue

Classical approaches to fatigue design involve the characterization of total fatigue life to failure in terms of the cyclic stress range (the S-n curve approach) or the (plastic or total) strain gauge. The total fatigue life is defined as the sum of the number of cycles to initiate a fatigue crack and the number of cycles to propagate it subcritically to some final crack size. In these methods, the number of stress or strain cycles necessary to induce fatigue failure in initially uncracked (and nominally smooth-surfaced) laboratory specimen is estimated under controlled amplitudes of cyclic stresses or strains. The resulting fatigue cycles to initiate a dominant crack (which can be as high as some 90% of the total fatigue life) and to propagate this dominant flaw until catastrophic failure occur.

Under high-cycle, low stress fatigue situations, the material deforms permanently elastically, the failure time or the number of cycles to failure under such high-cycle fatigue has traditionally been characterized in terms of the stress range. However, the stress associated with low-cycle fatigue are generally high enough to cause appreciable plastic deformation prior to failure. Under these circumstances, the fatigue life is characterized in terms of the strain range.

1.4. Defect-Tolerant Approach

The fracture mechanics approach to fatigue design, on the other hand, involves a "defect-tolerant" philosophy. The basic premise here is that all engineering components are inherently flawed. The size of pre-existing flaw is generally determined from nondestructive flaw detection techniques (such as visual, dye-penetrant, X-ray technique, ultrasonic, magnetic or acoustic emission methods). If no flaw is found in the component, or no cracks are detected by the NDT, the initial crack size is estimated from the resolution of the flaw detection technique. The useful fatigue life is then defined as the number of fatigue cycles or time to propagate the dominant crack

from the initial size to some critical dimension. The prediction of crack propagation life using the defect-tolerant approach involves empirical crack growth laws based on fracture mechanics.

1.5. Mechanistic Approach

Fatigue provides a broad variety of complex mechanistic processes for scientific investigation. The size scales of observation that are of interest in research area range from submicrostructural (even atomistic) levels to dimensions of structural components spanning tens or hundreds of meters. Even though the practical aspects of structural investigation in engineering components are important in fatigue studies, mechanistic and scientific basis for the study of the fatigue cannot be ignored because of the following reasons.

(a) The size scale over which highly intense damage occurs at the tip of fatigue crack is generally comparable to the characteristic microstructural dimension of the material, even if the component dimensions and the crack size are order of magnitude larger than the scale for the microstructure.

(b) The concepts of low-cycle fatigue and fracture mechanics provide methods for characterizing the resistance of the material to crack initiation and growth under cyclic loads, provided there exists a thorough understanding of the micromechanisms of failure.

(c) A significant portion of the fatigue crack growth life is spent at low ΔK levels where the maximum crack tip opening displacement during a loading cycle is typically smaller than a micrometer for microstructural components.

(d) "Post-mortem" analyses of fatigue failure often involves tracing the origin of fatigue failure via microscopic features present on the fracture surfaces, such as markings and striations. These features can provide valuable information about the location where

fracture initiated as well as above the magnitude of loads imposed upon the failed components.

1.6. A Comparison of different approaches to fatigue

The different approaches to fatigue also provide apparently different guidelines for the design of microstructural variables for optimum fatigue resistance. These differences are merely consequences of the varying degrees to which the role of crack initiation and crack growth are incorporated in the calculation of useful fatigue life. For example, in many structural alloys, the resistance to the growth of long fatigue cracks generally increases with an increase in grain size (or decrease in yield strength) at low ΔK values where a significant portion of subcritical crack growth life is expanded. On the other hand, the total fatigue life estimated on the basis of stress-life plots generally exhibits the opposite trend; higher strength materials and finer grained microstructures usually lead to a longer fatigue life.

The apparent contradiction between the two approaches can be reconciled by noting that the former approach to fatigue deals primarily with the resistance to fatigue crack growth, while the latter approach based on nominally defect-free laboratory specimens focusses mainly on the resistance to fatigue crack initiation. The choice of a particular microstructural condition for improvised fatigue life is then predicted upon the design philosophy for a specific application. Optimization of microstructural characteristics for improved resistance to both crack initiation and crack growth would require a trade-off between the two approaches.

1.7. Purpose of Present Research

The purpose of present research on fatigue damage assessment of FCC metals and alloys is to investigate cyclic deformation and fatigue fracture of these materials in an attempt to

determine the fracture life. The main approach adopted here focusses attention on scientific concepts and mechanisms of cyclic deformation. The following objectives would be achieved from this research work;

1. An integrated and quantitative treatment of the physics and micro-mechanisms of cyclic deformation, crack initiation and crack growth by fatigue.
2. A unified scientific basis for understanding the fatigue behaviour of polycrystalline FCC metals and alloys.
3. A balanced perspective of the various approaches to fatigue, with a critical analysis of the significance and limitations of each approach.

With the above objectives achieved, advice could be offered to local industrial establishments and small factories which use large quantity of face-centred cubic metals (such as Al, Cu, Pb, Au, Ag, Ni, Si etc) and their alloys. For instance, Al and Al-alloys are used as roofing sheets and cooking pans, while Cu is used in electrical works and α-Brass (Cu-30%Zn) is used as bushings in most machines. In many of these applications, the metal or alloy is subjected to repeated application of stress below the yield strength of the material. Even though the stress is below the yield strength, the material may fail after a large number of the repeated application of the stress (thermal or corrosion).

CHAPTER TWO

SPECIMEN DESIGN, FABRICATION AND PREPARATION

2.1. Selection of FCC Metals and Alloys

Most of the investigation carried out in fatigue are centred on engineering structures and components (such as connecting rods, stub axles, leaf springs, gear teeth, turbine blades, structural joints of various types, tail shaft of motor vehicles, coil springs, splined driving shafts, propellers of helicopter etc) [12]. In order to assess the damage caused by fatigue in FCC metals and alloys, commercial pure aluminium, pure copper, alpha brass, 0.25%C steel (mild steel) and 18Cr-8Ni stainless steel were selected for the following reasons. Cu-Cu-based alloys produce extensive cavitation during deformation. The selected FCC metals and alloys are used in fabricating engineering structures and components such as shaft, bolts and nuts which are frequently subjected to repeated stress. Selected FCC metals and alloys have a minimum of nonmetallic inclusions and thereby promote fatigue failure.

2.2. Selection of Testing Procedure

Generally, there are five main groups of fatigue testing machines designed to suit the type of fatigue loadings to which, parts are subjected in service [12]. The principles in each case are shown in Fig. 1 and the classification being related to the basic type of strain action or loading system which is applied to the specimen i.e. (rotating bending, plane bending, axial loading, torsion and combined stress).

In each group the machine may be of either constant load types eg. dead weight and centrifugal force, or constant displacement types eg mechanical displacement and constant strain. The method of loading can further be classified as mechanical, hydraulic, electromagnetic or

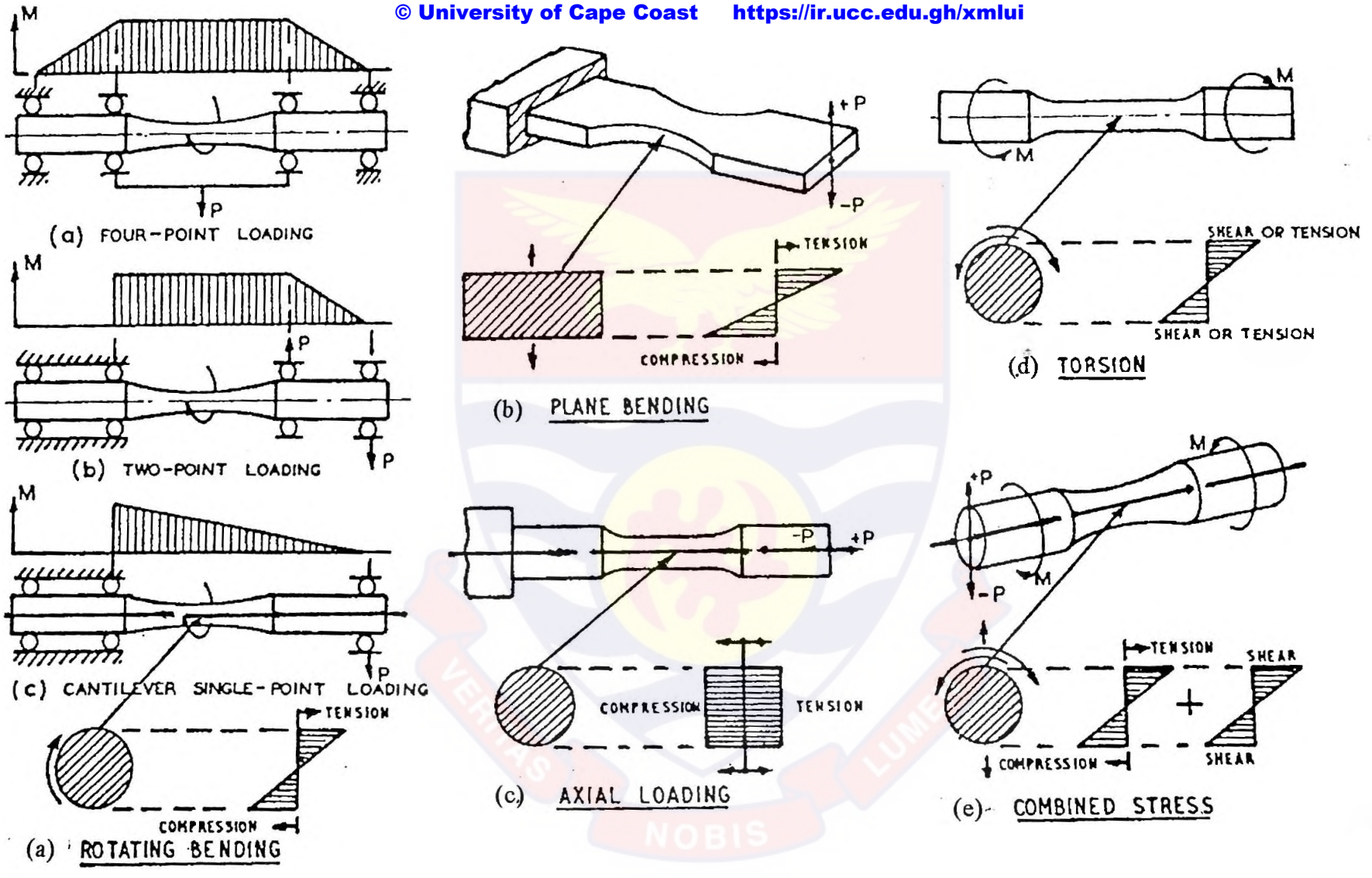

Fig. 1: Principles of fatigue testing machines [(a)-Rotating Bending, (b)-Plane Bending (c)-Axial Loading, (d)-Torsion, (e)-Combined Stress].

pneumatic and also whether or not they operate under near resonance conditions.

The rotating-bending cantilever machine (Fig. 1a) has been used extensively by researchers in the area of fatigue investigation. This appears in three forms, namely, one point, two point and four point loading. The test specimen is rotated under a bending load, as a consequence, each point on the surface is alternately stressed in tension and compression. In other types of machine, the specimen is held stationary and a revolving load used to obtain the desired stress conditions. Generally, the machine operates at frequencies within the range of 100 to 500 Hz.

In plane bending and axial loading machine (Fig. 1(b) and 1(c)) the mean stress is non -zero and the alternating load can be superimposed upon a static mean load to provide information which is applicable to many design problems. The frequency of such machines is less than 50 Hz but modern ones operate at frequencies higher than 300 Hz.

The torsional loading machine (Fig. 1d) produces both zero and non-zero mean stress conditions and has the maximum stresses occurring at the surface and a stress gradient which decreases from the surface to the centre of the specimen.

The combined stress machine (Fig. 1e) has been designed to suit engineering components and structures that are subjected to complex loading systems, such as combinations of either axial and bending loads or bending and torsional loads. Research work carried out with the machine is centred on the crankshaft of internal combustion engines and helicopter blades.

After describing the various types of fatigue testing machines as shown in Fig. 1, it was decided to use the rotating-bending cantilever single point loading fatigue machine which was available in the research laboratory at the Mechanical Engineering Department, University of Science and Technology, Kumasi. This machine is commonly known as Duplex type Fatigue Machine.

2.3. Specimen Design Parameters and Stress Calculations

2.3.1. Designing of Specimen

The standard test piece for the Duplex machine is shown in Fig.2 and is described commonly as Wohler test specimen. In the design, the cross section of the test piece is varied along the length in such a manner that the maximum stress occurs at MN (see Fig.2). The total applied load always acts downwards and rotates at a constant speed of 50 Hz. The stress changes sign every half revolution and the number of cycles of stress is equal to the number of revolutions of the machine.

2.3.2. Stress Calculation

The applied stress, σ, was calculated by using the equation 2.1 from a manual on fatigue machine at the Mechanical Engineering Department, U.S.T, Kumasi.

$$\sigma = \frac{(W \times L)}{Z} \qquad (2.1)$$

where Z is the section modulus of specimen (m^3), ($Z=\pi D^3/32$, D is the specimen diameter), W is the total load applied (in N), i.e the sum of the weight of load pan (W_1) and added weight (W_2), and L= 0.102 m is fixed length between the gauge diameter and threaded end of specimen. With D= 0.008 m at A (Fig 2) and W_1 = 22 N, the stress applied, σ (MPa), on the specimen is given by

$$\sigma = 2.04(22 + W_2) = 2.04W \qquad (2.2)$$

The calculated values are shown in Table 1

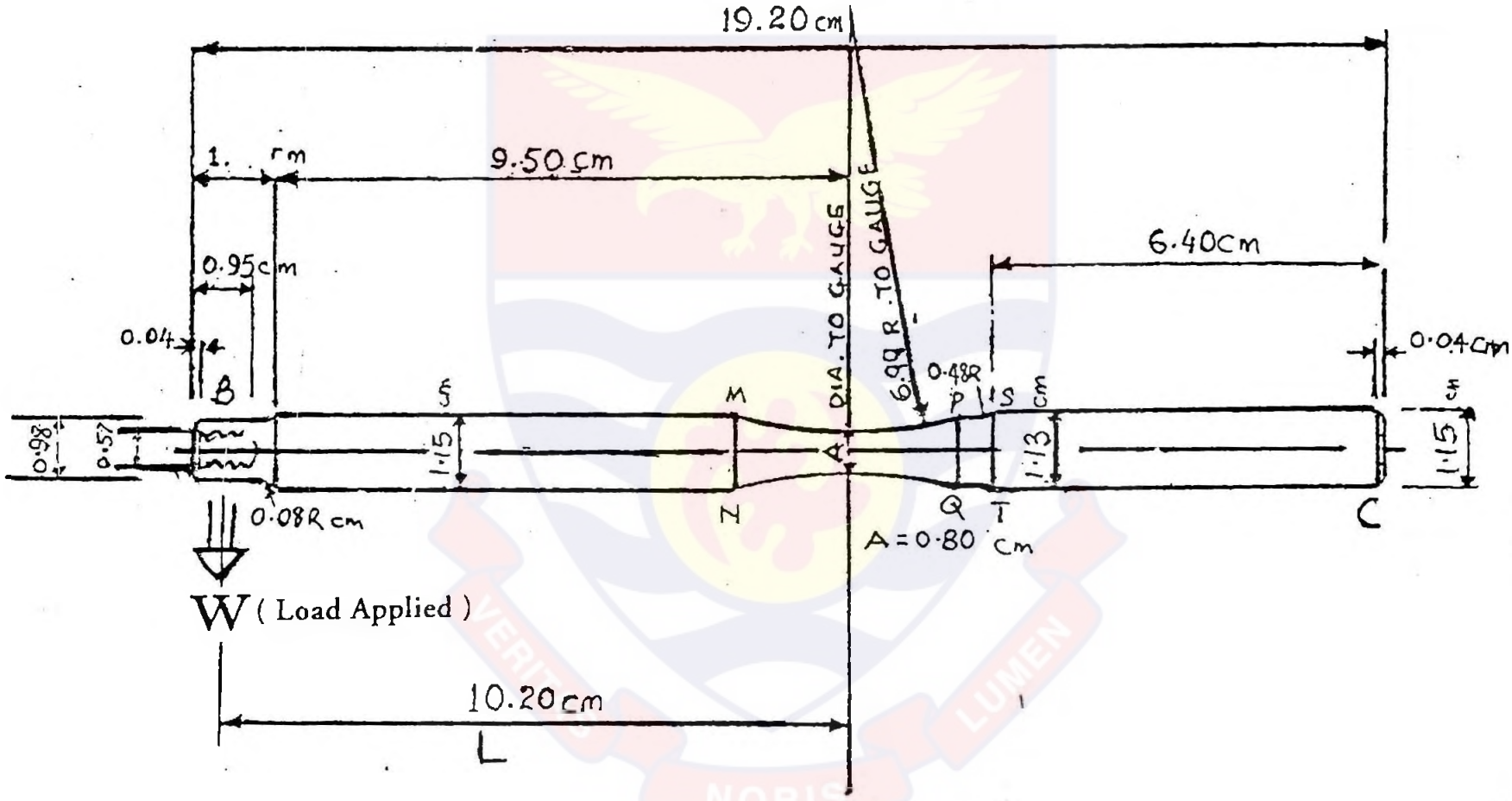

Fig. 2: Standard Test Piece for Duplex Fatigue Testing machine

Fig.2: Standard Test Piece for Duplex Fatigue Testing machine

Table 1 : Calculated Stress Levels for Wohler Specimens.

W_2 (N)	W (N)	σ (MPa)
8.8	30.8	62.9
22.0	44.0	89.8
44.0	66.0	134.7
66.0	88.0	179.6
88.0	110.0	224.5
110.0	132.0	269.4
132.0	154.0	314.3
154.0	176.0	359.2
176.0	198.0	403.9

Table 2 : Heat Treatment of Specimens.

Material	Melting Point T_m (K)	Annealing Temperature (K)	Annealing Time (h)
Al (pure)	933	733	3
Cu (pure)	1356	1123	2
Cu-30% Zn	1193	973	6
Mild steel (0.25%C)	1223	923	2
18 Cr-8Ni Stainless Steel	1573	1323	1

2.4. Specimen Fabrication

For the fatigue test, cylindrical rods of diameter 1.27 cm of the material were machined to attain a gauge diameter and length of 0.80 cm and 3.50 cm respectively. The length of specimen was 19.20 cm. With the exception of the gauge length, average diameter of specimen was 1.17 cm. Figure 3. shows as- fabricated fatigue test specimen.

Four (4) specimens were fabricated for each material to obtain S-n curve or stress -life plots at room temperature. Six (6) additional specimens were fabricated to investigate fatigue dependance on temperature range from 300 - 800 K.

2.5. Heat Treatment

Heat treatment is an operation involving the heating of a solid material to a definite temperature, followed by cooling at suitable rate, associated with changes in the nature, form, size and distribution of microconstituents [13 - 16]. Specimens were annealed in a furnace at different temperatures and times in order to produce ductility, homogeneity of structure, large grain sizes and minimize internal stresses. The annealing was done in an inert atmosphere of argon to prevent oxidation of the specimens [17].

After heating for the specified time, each specimen was then cooled in air to room temperature and stored in a desiccator to prevent oxidation. Table 2 shows the heat treatment conditions. The annealing temperatures were selected to be lower than the melting point (T_m) by at least 200 K.

2.6. Mechanical Polishing and Surface Treatment

Emery paper of gritsize ranging between 60 and 500 were used for the mechanical polishing. Grit size 60 was initially applied and stepped up to 80, 100, 120 and finally polished to mirror finish using grit-size 500. Further polishing was done using Textmet cloth and alumina powder, so that final polishing was done to 0.5 μm alumina powder.

Fig.3: As-fabricated fatigue test specimen

CHAPTER THREE

MICROSTRUCTURAL EXAMINATION AND FLAW DETECTION OF UNTESTED (FABRICATED) SPECIMENS

3.1. Grain Size Determination

3.1.1. Specimen Preparation

Samples were mechanically polished on silicon carbide polishing paper, by following the following procedures. The first stage of the polishing procedure was by using gritsizes of 240, 320, 400 and 600 respectively. At each stage, polishing was done until all the scratches from the preceding one were gone. This was achieved by passing the specimen in the same direction on each paper, so as to have all the scratches parallel and then to rotate the specimen 90 degrees when changing to the next paper.

Finally samples were washed thoroughly in alcohol and the surface dried by using hot air blower.

3.1.2. Etching

Etching is the process by which the grains in a material are selectively attacked and thereby reveal the grain boundaries as dark network [18]. For the aluminium specimen to achieve grain contrast, the etchant used was 5 ml HNO_3, 2 ml HF and 100 ml H_2O at an etching time of about 30 seconds. For grain contrast in the Copper specimen, 25% NH_4OH and five drops of H_2O_2 was used, and the etching period was about 30 seconds. To obtain the grain contrast in Cu-30%Zn, a mixture of 50 ml of HNO_3 and 50 ml H_2O was used, and the etching period was 5 seconds . Mild steel attain grain contrast after etching with 2 ml HNO_3 and 98 ml C_2H_5OH for about 5 seconds. Finally Stainless steel; was etched with 50 ml HCl for a period of about

3 minutes to attain grain contrast.

3.1.3. Optical Microscopy Examination

An M41 Photoplan microscope with an automatic exposure unit under the reflection mode was used for the observation and counting of grains. The graticule of the eyepiece was calibrated by using a magnification of 10X for the objective so that, the full length of graticule corresponds to 1000 μm. Polished and etched samples were placed on microscopic slide and firmly held by plasticine and mounted under the microscope for observation. At focus, the number of grains crossing the entire length was counted and recorded. The mean linear intercept grain size [14] was found by dividing the entire length of graticule by the mean number of grains. More than 250 grains were measured to obtain the average grain size, d, (equivalent to 1.74 x $\bar{L}$, where $\bar{L}$ is the mean linear intercept grain size). An optical micrograph of an etched Cu showing the grain distribution and grain boundaries is shown in Fig.4. A plot of statistical scatter on the average values of grain size d against total number of readings η is shown in Fig.5.

The statistical scatter on the average value of the grain size off set was determined at the 95% confidence level from the following equation [19],

$$\%Scatter = 1.96 \frac{(\Sigma d^2 - \Sigma(\frac{d^2}{\eta}))}{(\eta-1)\ (d\sqrt{\eta})} \qquad (3.1)$$

where η is the total number of readings taken, and d is the mean value of the grain size offsets. The scatter decrease with an increase in the number of readings levelling off to < 10% for $\eta \geq 250$ as shown in Fig.5.

Fig.4. Optical micrograph of an etched Cu showing the grains and grainboundaries.

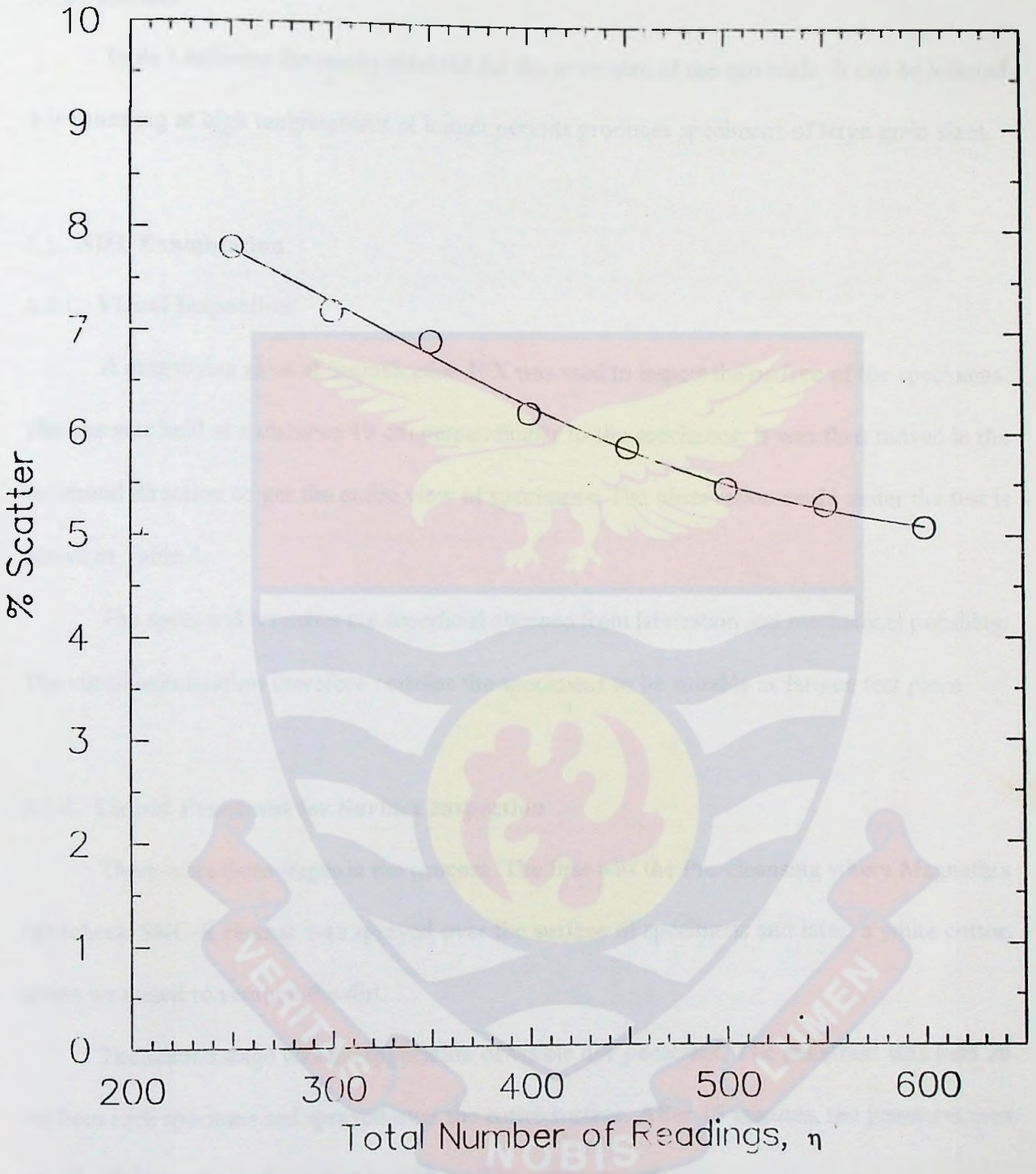

Fig.5. Plot of %Statistical Scatter on the average value of grain size against total number, η of Readings.

3.1.4. Results

Table 3 indicates the results obtained for the grain size of the materials. It can be inferred that annealing at high temperatures at longer periods produces specimens of large grain sizes.

3.2. NDT Examination

3.2.1. Visual Inspection

A magnifying glass of magnification 10X was used to inspect the surface of the specimens. The lens was held at a distance 10 cm perpendicular to the specimens. It was then moved in the horizontal direction to get the entire view of specimens. The observation made under the test is shown in Table 4.

The spots and scratches are superficial obtained from fabrication and mechanical polishing. The visual examination therefore certifies the specimens to be suitable as fatigue test piece.

3.2.2. Liquid Penetrant for Surface Inspection

There were three stages in the process. The first was the Pre-cleansing where Magnaflux Spotcheck SKC-S cleaner was sprayed over the surface of specimens and later, a white cotton gauze was used to remove the dirt.

The second stage was the application of visible dye penetrant. The penetrant was held 30 cm from each specimen and sprayed over the entire surface. After 15 minutes, the penetrant was wiped off the surface of specimens with a white cotton gauze.

For the final process, a developer in the form of suspension was shaken for few minutes and sprayed thinly over specimens and left for 10 minutes. No cracks were observed when viewed through the developer, hence confirming the results of visual inspection.

Table 3 : Grain sizes of the materials

Material	Grain Size, d (μm) ± 10%	Annealing Temperature (K)	Annealing Time (h)
Al (Pure)	72.5	733	3
Cu (Pure)	341.2	1123	2
Cu-30% Zn	150.0	973	6
Mild steel (0.25%)	63.5	923	2
18Cr - 8Ni Stainless steel	45.0	1323	1

Table 4 : Visual Observation of Fabricated Specimens.

Material		Observation of Surface Flaws
A1	A1	Tiny dark spots around surface
	A2	Few scratches
	A3	Tiny dark spots around surface
	A4	Pronounced scratches
Cu	K1	Tiny dark spots and scratches
	K2	Few scratches
	K3	Tiny dark spots and scratches
	K4	Tiny dark spots and scratches
Cu- 30%Zn	B1	Tiny dark spots and scratches
	B2	Tiny dark spots and scratches
	B3	Few scratches
	B4	Tiny dark spots and scratches
Mild Steel (0.25%C)	M1	Pronounced dark spots
	M2	Pronounced dark spots
	M3	Pronounced dark spots
	M4	Pronounced dark spots
18 Cr-8Ni Stainless Steel	S1	Dark spots
	S2	Dark spots and few scratches
	S3	Pronounced dark spots and scratches
	S4	Tiny dark spots and scratches

3.2.3. Radiography Examination for Internal Flaw Detection

For radiographic examination, the exposure is measured in (mA-min) and depends on the thickness of the material. Exposure Chart which relates exposure to thickness has been prepared on types of steel as shown in Fig.6 [20]. For this chart to be used for other materials , references was made to equivalent chart [21] to get the equivalence thickness of steel and hence the exposure for the materials as shown in Table 5.

With the exception of α-brass and Cu which an energy of 230 kV was used, 170 kV was used for the other materials at a current setting of 2 mA. After the specimens had been exposed for various times, the exposed films were developed, fixed and examined by a high intensity film viewer to check for internal discontinuities in the specimen. Results obtained from the radiographic examination are indicated in Table 6.

No part of the film was found to be darkened more than the other, which is an indication that no defect is present and X-ray radiation absorption was high in all areas [18]. Furthermore, for any good film, the recommended density should lie between the range of 1.8 and 4 [22]. Since the densitometer readings were within the range, the selected exposure factors used for the investigations were good.

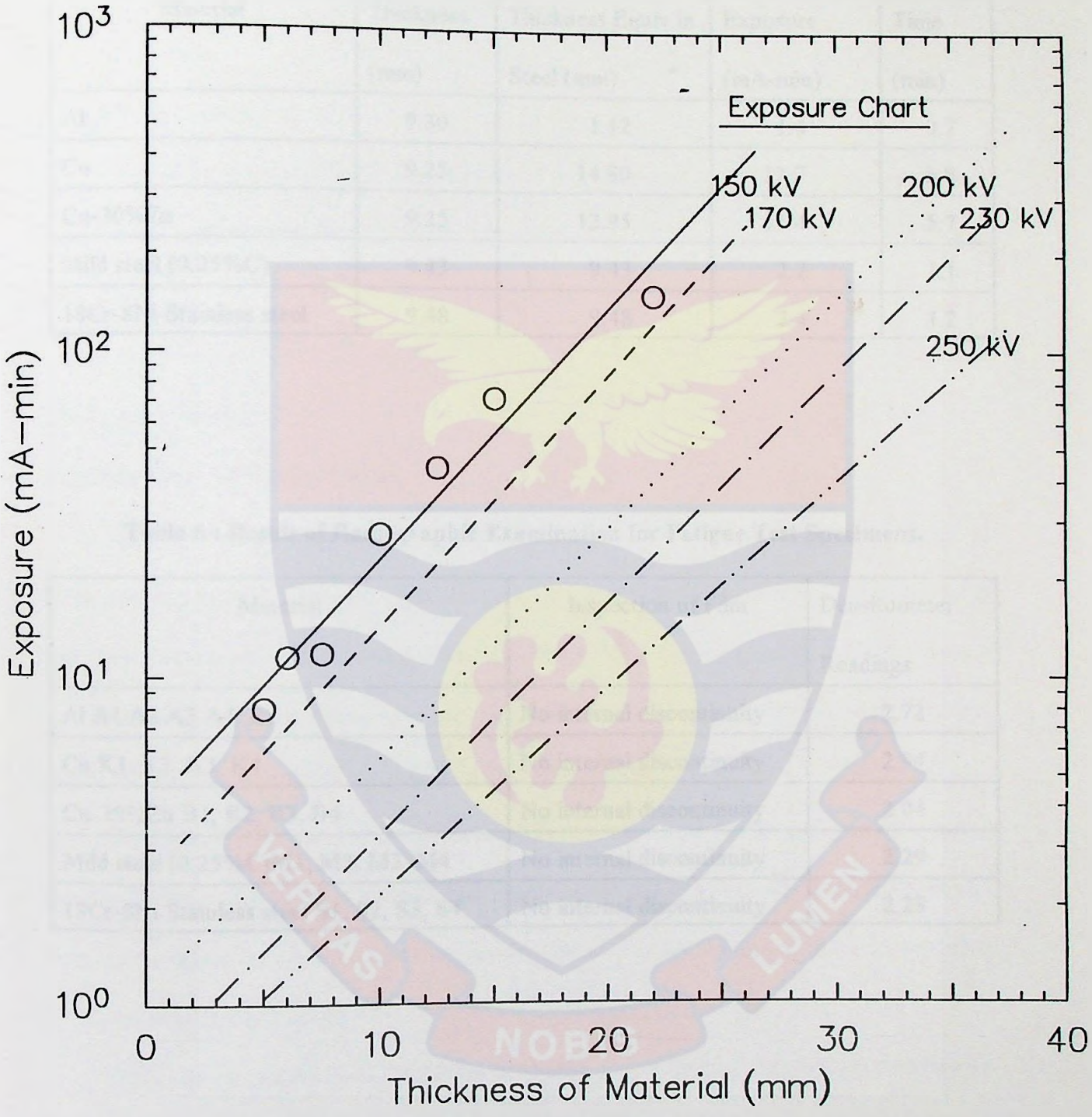

Fig.6. Exposure Chart for Steel

Table 5 : Exposure Table for Fatigue Test Specimens.

Material	Thickness (mm)	Thickness Equiv in Steel (mm)	Exposure (mA-min)	Time (min)
Al	9.30	1.12	1.4	0.7
Cu	9.25	14.80	12.7	6.8
Cu-30%Zn	9.25	12.95	11.4	5.7
Mild steel (0.25%C)	9.43	9.43	2.2	1.1
18Cr-8Ni Stainless steel	9.48	9.48	2.4	1.2

Table 6 : Result of Radiographic Examination for Fatigue Test Specimens.

Material	Inspection of Film	Densitometer Readings
Al A1 A2 A3 A4	No internal discontinuity	2.72
Cu K1, K2, K3, K4	No internal discontinuity	2.94
Cu 30%Zn B1, B2, B3, B4	No internal discontinuity	2.04
Mild steel (0.25%C)M1, M2, M3, M4	No internal discontinuity	2.29
18Cr-8Ni Stainless steel S1, S2, S3, S4	No internal discontinuity	2.28

CHAPTER FOUR

MECHANICAL TESTING

4.1. Introduction

To obtain data on ductility and strength of the specimens, impact tests were performed to evaluate the different materials and set up appropriate links of stresses to be used in the fatigue tests.

4.2. Impact Testing

4.2.1 Relevance of Impact Testing

Impact testing is used in studying the ductility of a material in terms of energy absorbed during fracture. In static tensile test, this energy is represented by the area under the stress-strain diagram and can therefore be concluded that, in order to have high toughness, the material must have high strength and at the same time large ductility. Materials that are brittle normally have low toughness and as such exhibit small deformation before fracture.

At higher temperatures, a material behaves in a ductile manner with extensive deformation observed before fracture [23]. A material that may be subjected to an impact blow during service must have a brittle-ductile transition temperature, below the temperature of the surroundings if it is to undergo brittle fracture.

Notches caused by poor machining or design act as stress concentrators and thereby reduce the toughness of the material. The notch sensitivity of a material can be evaluated by comparing the energies of the notched and un-notched specimens. The absorbed energy and the brittle-ductile transition temperature are sensitive to the loading condition. For example the rate at which energy is applied to the specimen will reduce the absorbed energy and increase the

transition temperature.

Finally, the configuration of the material may affect the behaviour. A surface crack permits lower absorbed energies than a v-notch. Since all the conditions cannot be predicted or controlled the Impact Test is used for comparison and selection of materials rather than as design criterion [23, 24].

4.2.2. Impact Test Pieces (un-notched and notched)

For the Impact Test, notched and un-notched samples of dimension 1 cm x 1 cm x 6 cm were produced for each material by using a shaper machine. The notched specimen was fabricated to produce at the centre a v-notch of 1 mm in length with an opening angle of 45 degrees as shown in Fig.7.

4.2.3 Description of Impact Testing Machine

The Impact Testing Machine shown in Fig.8 combines in one unit the facility for making tests on metallic materials in three recognized ways: i.e cantilever or "Izod" test, beam or "charpy" test, and Impact tension test. The machine has capacity ranging from 0 to 160 J.

Two control levers are fitted; one for releasing the pendulum and the other for clamping the specimen. The impact value of the test piece is read on the dial gauge which has a maximum recording pointer. A stop is fitted to support the pendulum in the rest position.

Two ratchets are fitted to the pendulum to locate it at 160 J height. The pendulum is held in position by toggles operated by the left-hand lever at the front of the machine.

4.2.4. Testing Procedure

The striker of the impact testing machine shown in Fig.8 was fitted with the horizontal

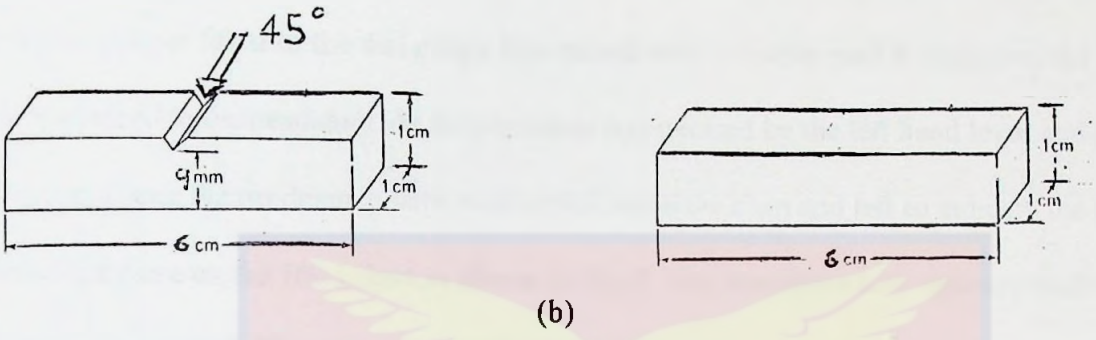

(a) (b)

Fig.7. Impact Test Specimen: (a) V-notch, (b) Un-notched

Fig.8. Impact Test machine

top in the striking position. After positioning the grips, the test pieces with notch were inserted such that the notch turned to the right and correct height set with the setting gauge on top of the right hand grip. Grips were then locked and with the pendulum raised to 160 J position, the maximum pointer fitted to the dial gauge was turned anticlockwise until it contacted the fix pointer attached to the pendulum. As the pendulum was released by the left hand lever and passed on the test pieces, the maximum pointer was carried round the chart and left to indicate the impact value of test piece on the 160 J chart as shown in Fig.8. The procedure was repeated until failure of test piece occurred. The accrued energies for failure were used as the static fracture energies for specimens.

4.3 Fatigue Tests

4.3.1 Description of Dynamic Fatigue Testing Machine

There are many forms of fatigue tests which make use of different machines and specimens as shown in Fig. 1 but the present investigation is centred on the use of Duplex Testing Machine which belongs to the class of rotating bar fatigue testers. The machine is suitable for determining alternating bending stress based on the principles laid down by Wohler [12]. Considering σ_{max} and σ_{min} as the maximum and minimum values respectively of the repeated stress, their algebraic difference becomes the range (σ_r) of the stress, i.e.,.

$$\sigma_r = \sigma_{max} - \sigma_{min} \qquad (4.1)$$

The fatigue cycle is completely defined if the range and the mean stress are given, where the average or mean stress is expressed as

$$\bar{\sigma} = \frac{(\sigma_{max} + \sigma_{min})}{2} \qquad (4.2)$$

For reversed stress, $\sigma_{min} = -\sigma_{max}$ and hence by substituting this relation into eqn (4.1)and (4.2), the results become $\sigma_r = 2\sigma_{max}$ and $\bar{\sigma} = 0$.

A fatigue cycle of varying stress can therefore be obtained by superposing a cycle of reversed stressed on a steady average stress. From eqns. (4.1) and (4.2), the maximum and minimum values of the varying stres are given as

$$\sigma_{max} = \bar{\sigma} + \frac{\sigma_r}{2} \qquad (4.3)$$

$$\sigma_{min} = \bar{\sigma} - \frac{\sigma_r}{2} \qquad (4.4)$$

The Duplex fatigue machine (Fig.9) consists of a cast iron housing the specimens at each end of the shaft. The stress cycle counter coupled to the motor starter of the machine records the number of stress reversals for each specimen. One cycle of the pointer of clock indicates 10^7 reversals.

A button cut-out contact is set under the centre of the load pan so that it drops upon the cut-out contact, thereby breaking the circuit of its stress cycle counter. The shaft of the motor has a chuck which consists of a slotted collect which fits in a conical holder in the shaft end, and is pushed in by a nut. The collet is held by means of an open jawed spanner and the nut turned by

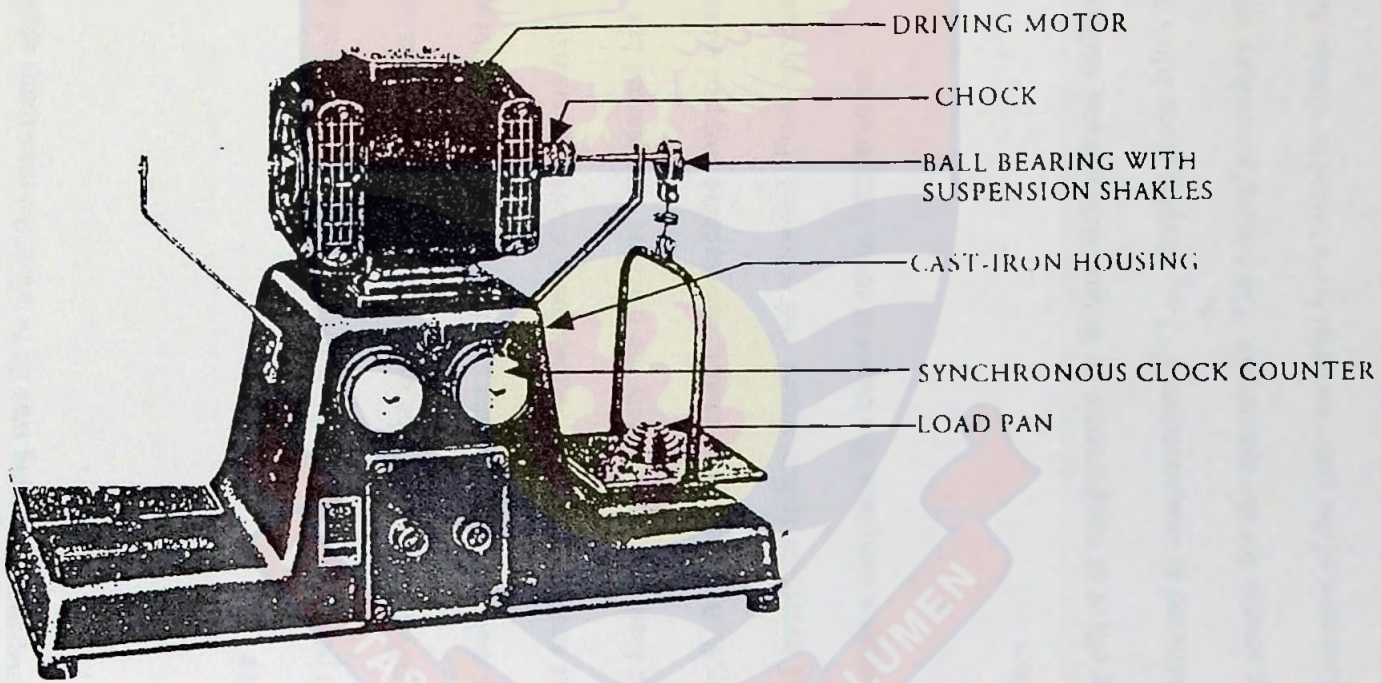

Fig.9. Duplex Fatigue Testing machine

means of "C" spanner while specimens were being secured.

A ball bearing with suspension shackles have been provided for fitting on the specimens at the prescribed distance from the gauge diameter. The test speed of the machine is 50 Hz and gauge diameter of standard specimen used (Fig.2) is 0.008 m respectively. The weight of the load pan of the machine and suspension bearing was 22 N while the maximum applied load was 196 N.

4.3.2. Testing Procedure

A ball bearing was pushed onto the outer end B of the cleaned and well greased specimen with threading and held firmly with a screw. The outer end C of the specimen was firmly secured in the chuck of the Duplex machine under rotating cantilever single point loading. Pre-determined load was then placed in the scale pan to obtain a maximum stress. To ensure proper suspension, support was given to the load pan immediately the machine was started but quickly removed thereafter as shown in Fig.9. At the point of failure, the machine stopped automatically and the corresponding number of cycles to failure noted and recorded. Four specimens of the same material were tested to obtain a complete S-n curve at room temperature.

4.3.3. Temperature Effect

To investigate the effect of temperature on fatigue strength and endurance limit cycles, additional tests were conducted at temperatures $T<T_{m/2}$, ranging from 300 - 700 K by using a mini-furnace as a heating source for the specimens. The testing procedure was the same as in section 4.3.2. About six specimens of the same material were tested to obtain data for the plot of temperature on fatigue strength and endurance limit cycles.

The Kanthal wound-ceramic furnace, based on the design criteria of Laubenit [25] and

constructed by Quainoo [26] was used. The furnace had a 2.5 cm internal diameter and 4.8 cm external diameter of ceramic pipe of length 6 cm. The length of the ceramic pipe was divided into three section each of 2 cm. The Kanthal wire (diameter 0.4 mm, resistivity 11.20 Ωm, max operating temperature 1473 K) was made into a coil of about 50 cm long and wound on the length of ceramic pipe with three turns at the end sections and four turns at the central section of the pipe. The non-symmetrical winding on pipe was adopted to take care of radiation loses at the end of the furnace. The wires were then held in place by applying super glue to them. Upon drying, a paste of Kaolin (from Saltpond Ceramics) mixed with clay (as bonding material) was used to insulate the Kanthal wires on the outside of the pipe. This was then cased in a 6 cm diameter steel pipe of length 8 cm with two holes drilled on its size for the leads to come through them. Ceramic beads were used to insulate the leads of the Kanthal wires and then connected to porcelain connecter. The furnace was further insulated after casing. This was done by filling the remainder of the space of the ceramic winding and the steel pipe with more of the powdered Kaolin, to ensure that the wires did not touch the casing. Heat was suppllied to the furnace by means of a current regular temperature control device (transformer) through which current passed via the Regavolt variable A.C (VARIAC) transformer, type 402 Regasafe, with input voltage 240 V, 47-65 HZ, Output voltage 0-275 V and rated current 2.5 A. The secondary terminals of the transformer were connected to the porcelain connector and then to the furnace as shown in figure 10.

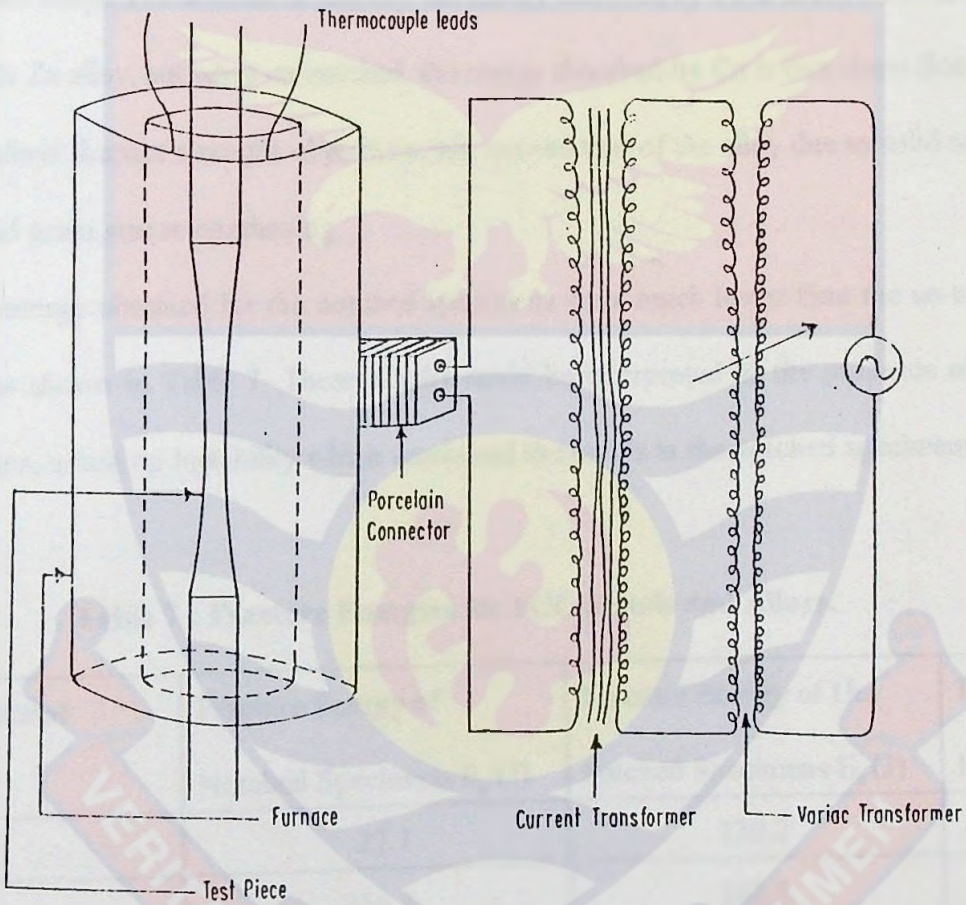

Fig. 10 Power supply to high temperature furnace.

CHAPTER FIVE

RESULTS AND DATA ANALYSIS

5.1. Results for Impact Testing

Table 7 indicates the fracture energy for both notched and un-notched specimens of the FCC metals and alloys. For notched specimens, the energy absorbed by Cu is about nine times that of the Cu-30% Zn alloy, but when un-notched, the energy absorbed by Cu is two times that of the Cu-30% Zn alloys. Impact strength of pure metals, exceed that of the alloy due to solid solution hardening and grain size strengthening.

The energy obtained for the notched specimens were much lower than the un-notched specimens as shown in Table 7. These results could be interpreted as the presence of stress concentrations, notch tip instability which weakened the bonds in the notched specimens and

Table 7 : Fracture Energies for FCC Metals and Alloys.

Material	Fracture Energy of Notched Specimens E_a (J)	Fracture Energy of Un-notched Specimens E_u (J)	Ratio E_u/E_a
Al	27.1	130.2	4
Cu	256.3	562.8	2
Cu-30% Zn	29.8	345.8	11
Mild steel (0.25% C)	71.9	271.2	4
18 Cr-8Ni stainless steel	130.2	424.4	3

hence the observed lower absorbed energy [12, 27, 28]. This results provided the clue for adequate preparation of the fatigue specimens to reduce the effect of stress concentrations,

surface cavities etc.in failure to the minimum.

5.2. Fatigue life-Analysis

5.2.1. Aluminium

Table 8 shows the results of the fatigue test conducted at room temperature for Aluminium. The corresponding Wohler S-n curves are shown in Fig. 11 and 12 from which it is deduced that the endurance limit or fatigue strength σ_e, is 173.3 MPa. Since the UTS for Aluminium is 542 MPa [12] the endurance ratio, σ_e /UTS = 0.32, which is comparable to the reported endurance limit and endurance ratio of 173.0 MPa and 0.32 respectively [12].

5.2.2. Copper

The results obtained for Copper under the same condition as Section 5.2.1 is indicated in Table 9. Fig.11 and 12 also represent the corresponding S-n curves from which the endurance limit σ_e, 62.9 MPa was deduced. The endurance ratio determined for Copper using its UTS value of 213.8 MPa was 0.29 which corresponds to the reported value of 0.29 [12].

5.2.3. Cu-30% Zn

Table 10 depicts the results obtained for Cu-30% Zn under the same conditions as the former. From the corresponding S-n curves in section 5.2.2, the endurance limit σ_e deduced was 97.0 MPa. The corresponding endurance ratio determined by using a UTS value of 309.6 MPa was 0.31 which is acceptable compared to reported value of 0.31 [12].

Table 8 : Fatigue Test Data for Aluminium at Room Temperature.

W_2 (N)	W (N)	σ (MPa)	No. of Cycles to Failure x 10^5 (Hz)
62.9	85.0	173.3	100
69.1	91.1	185.9	43
76.7	95.6	195.0	20
84.8	102.9	210.0	5

Table 9 : Fatigue Test Data for Copper at Room Temperature.

W_2 (N)	W (N)	σ (MPa)	No. of Cycles to Failure x 10^5 (Hz)
8.8	30.8	62.9	96
9.7	31.7	64.7	32.5
11.7	33.0	67.0	15
13.0	35.2	73.0	2

Table 10 : Fatigue Test Data for Cu-30%Zn at Room Temperature

W_2 (N)	W (N)	σ (MPa)	No. of Cycles to Failure x 10^5 (Hz)
25.5	47.5	97.0	80
27.3	49.3	100.6	25
28.6	50.6	103.3	12
33.9	55.9	114.0	3

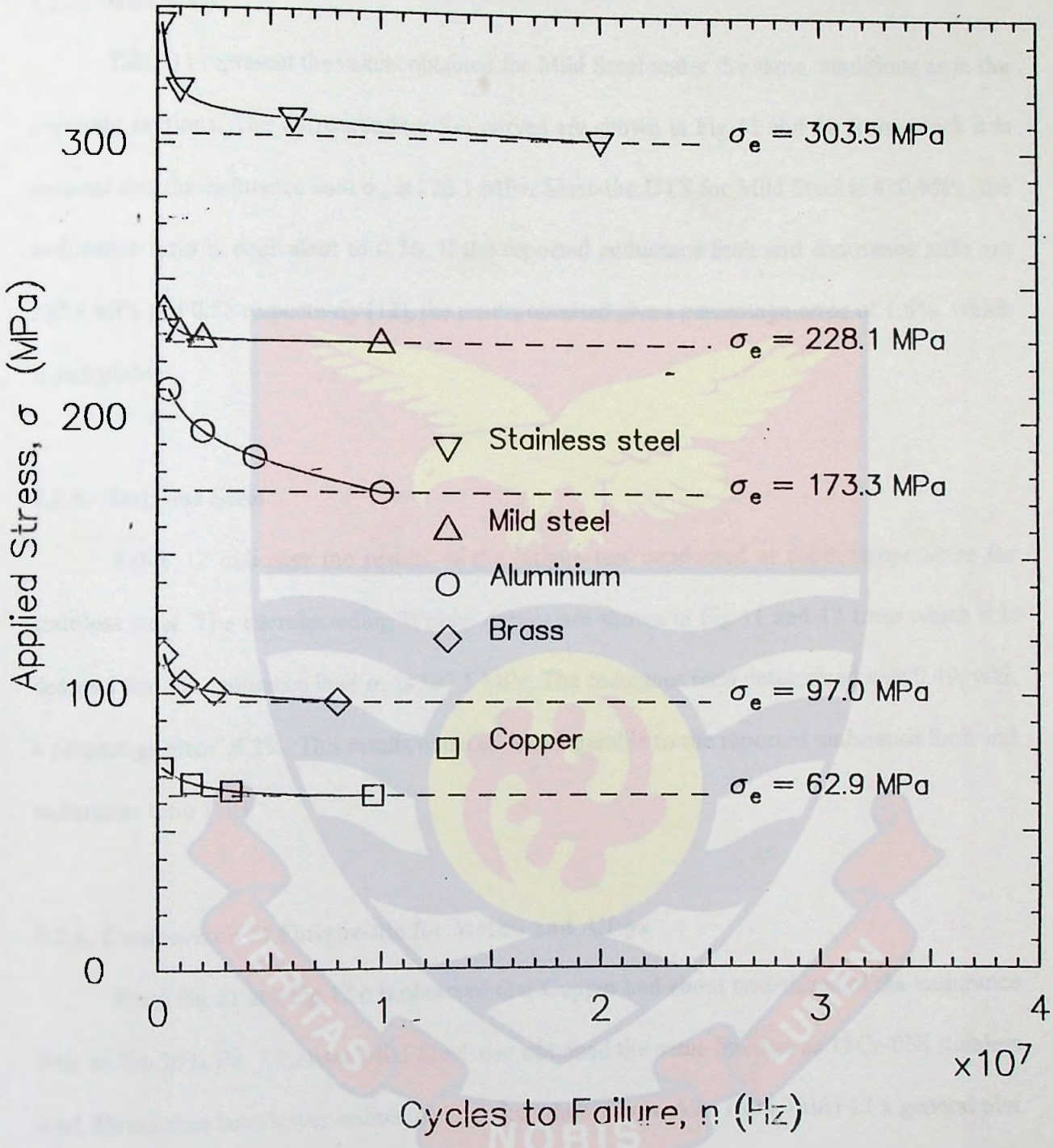

Fig. 11. Plot of Applied Stress versus Number of Cycles to Failure, n for FCC Metals and Alloys at Room Temperature.

5.2.4. Mild Steel

Table 11 represent the results obtained for Mild Steel under the same conditions as in the previous sections. The corresponding S-n curves are shown in Fig.11 and 12 from which it is deduced that the endurance limit σ_e is 228.1 MPa. Since the UTS for Mild Steel is 410 MPa, the endurance ratio is equivalent to 0.56. If the reported endurance limit and endurance ratio are 227.4 MPa and 0.55 respectively [12], the results obtained give a percentage error of 1.8%, which is acceptable.

5.2.5. Stainless Steel

Table 12 indicates the results of the fatigue test conducted at room temperature for stainless steel. The corresponding Wohler curves are shown in Fig.11 and 12 from which it is deduced that the endurance limit σ_e is 303.5 MPa. The endurance ratio determined was 0.49, with a percentage error of 2%. This results obtained is comparable to the reported endurance limit and endurance ratio [12].

5.2.6. Comparison of Fatigue-life for Metals and Alloys

From Fig.11 and Fig.12 it is observed that Copper had about two-thirds of the endurance limit of Cu-30% Zn. Likewise Mild Steel also obtained the same fraction as 18Cr-8Ni stainless steel. Metals then have lower endurance limit than their alloys. Also from Table 13 a general plot of fatigue strength against UTS for all specimen of different materials was made as shown in Fig.13. The gradient obtained was 0.52 which is acceptable comparing with the reported value of 0.50 [12].

Table 11 : Fatigue Test Data for Mild Steel at Room Temperature

W_2 (N)	W (N)	σ (MPa)	No. of Cycles to Failure (Hz) x 10^5
89.8	111.8	228.1	100-0
90.2	112.2	229.0	20-0
91.1	113.1	230.8	10-0
95.4	117.0	238.9	3-0

Table 12 : Fatigue Test Data for Stainless Steel at Room Temperature

W_2 (N)	W (N)	σ (MPa)	No. of Cycles to Failure x 10^5 (Hz)
126.7	148.7	303.5	200-0
129.8	151.8	309.8	60-0
134.6	156.6	320.0	10-0
147.0	169.0	344.0	2-0

Table 13 : Endurance limit, UTS and Endurance Ratio of the Specimens.

Material	σ_e (MPa)	UTS (MPa)	Endurance Ratio, σ_e /UTS
Cu	62.9	213.8	0.29
Cu-30% Zn	97.0	309.6	0.31
Al	173.3	542.2	0.32
Mild Steel(0.25% C)	228.1	410.0	0.56
18 Cr-8Ni Stainless Steel	303.5	613.3	0.49

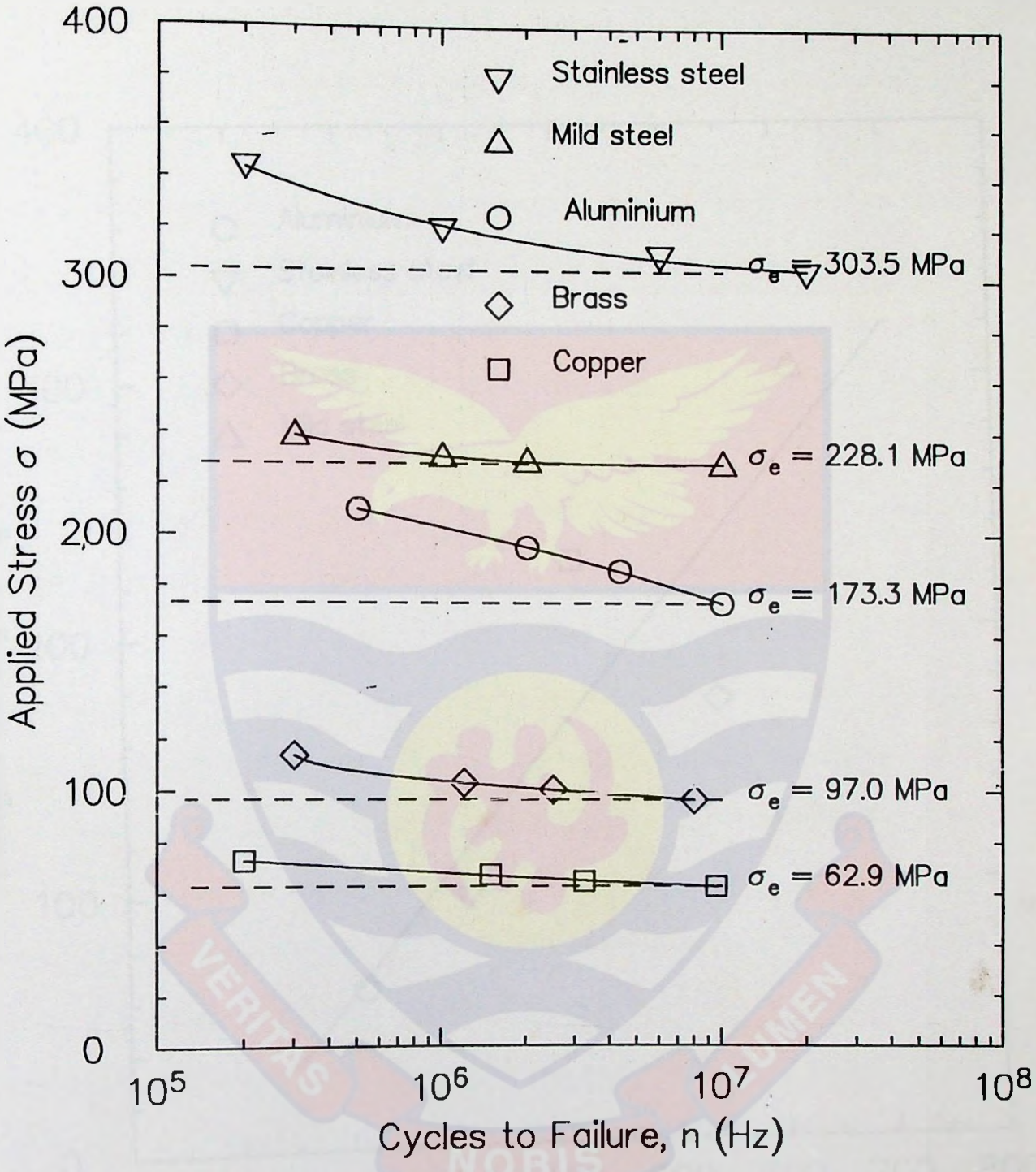

Fig. 12. Plot of Applied Stress versus log Number of Cycles to Failure, n of FCC Metals and Alloys at Room Temperature.

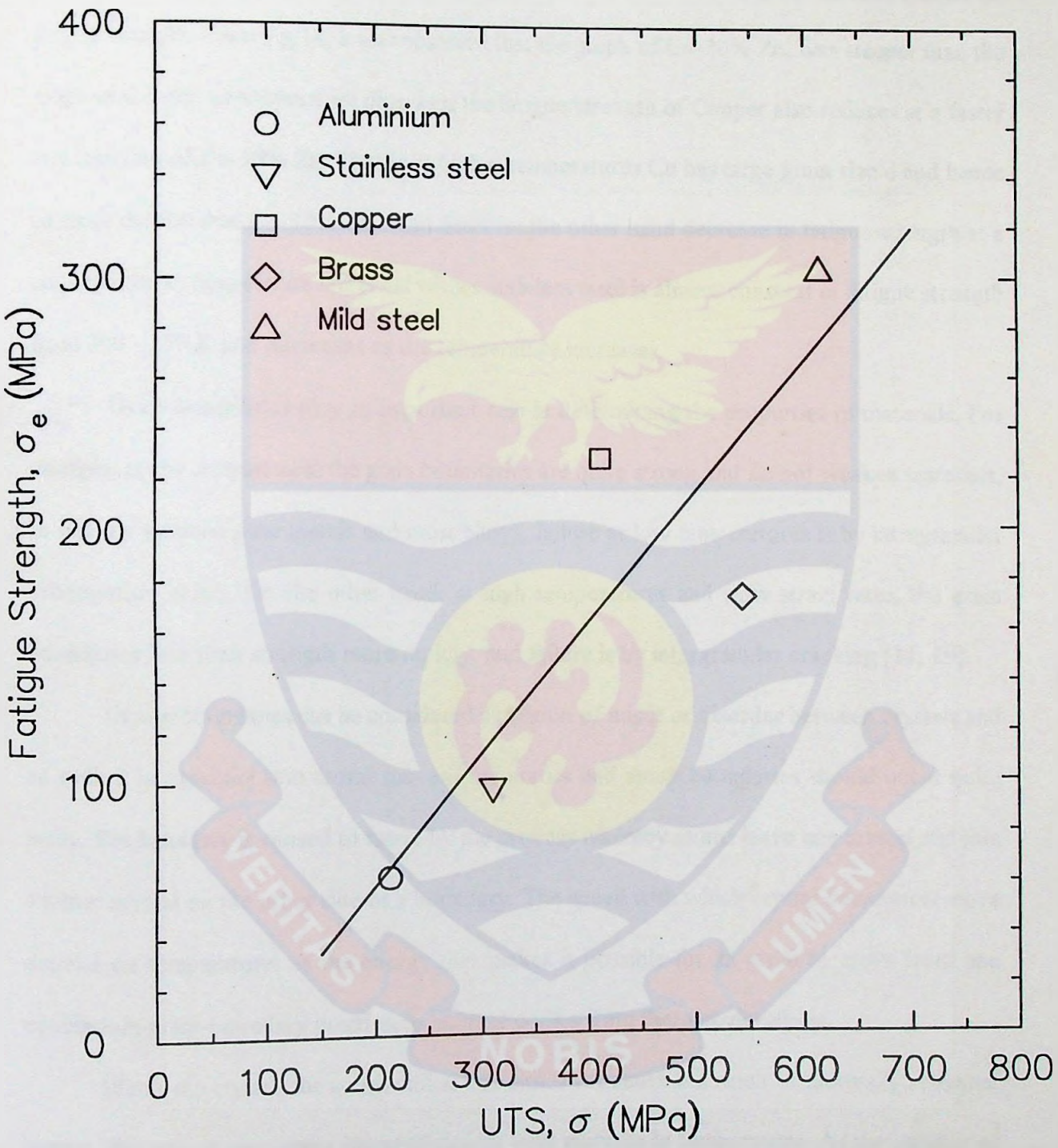

Fig. 13 Plot of Fatigue Strength versus UTS for FCC Metals and Alloys at Room Temperature.

5.3. Temperature Effect on Fatigue Strength

Table 14 and Fig. 14 represent the results obtained for the variation of temperature on fatigue strength. From Fig. 14, it was observed that the graph of Cu-30% Zn, was steeper than the graph of Copper, as temperature decreases the fatigue strength of Copper also reduces at a faster rate than that of Cu-30% Zn. That is at higher temperatures Cu has large grain size d and hence easier to deform than Cu-30% Zn. Mild Steel on the other hand decrease in fatigue strength at a constant rate as temperature increases whiles stainless steel is almost constant in fatigue strength from 300 - 350 K and decreases as the temperature increases.

Grain boundaries play an important role in determining the properties of materials. For example, at low temperatures the grain boundaries are quite strong and do not weaken materials. In heavily strained pure metals and most alloys, failure at low temperatures is by intragranular propagation crack. On the other hand, at high temperatures and slow strain rates, the grain boundaries lose their strength more rapidly and failure is by intergranular cracking [14, 29].

Crystal boundaries can be considered as region of misfit or disorder between crystals and as such it is expected that atoms movements across and along boundaries should occur quite easily. The boundary is caused to move by the process whereby atoms leave one crystal and join another crystal on the other side of a boundary. The speed with which crystal boundaries move depend on temperature: as the energy that makes it possible for an atom to move from one equilibrium grain-boundary position to another comes from thermal vibrations.

Within the crystals the atoms diffuse into lattice vacancies as a result of thermally activated jumps. The rate of movement increase rapidly with increase in temperature. As the number of atoms moving towards one direction becomes greater than the other, the energy of the material is lowered resulting in the movement of grain boundary. At this state the specimen moves into a

Table 14 Effect of Temperature on Fatigue Strength of Specimens

Temperature (K)	Fatigue Strength σ_c (MPa)				
	Aluminium	Copper	Cu-30%Zn	Mild steel	Stainless steel
303	173.3	62.9	97.0	228.1	303.5
323	168.5	60.8	96.0	220.5	301.4
373	157.4	58.8	92.9	204.7	299.4
423	138.8	45.0	81.1	199.8	285.6
473	92.5	33.0	67.4	190.2	273.8
573	74.5	-	26.1	179.2	232.5
673	-	-	-	-	209.5

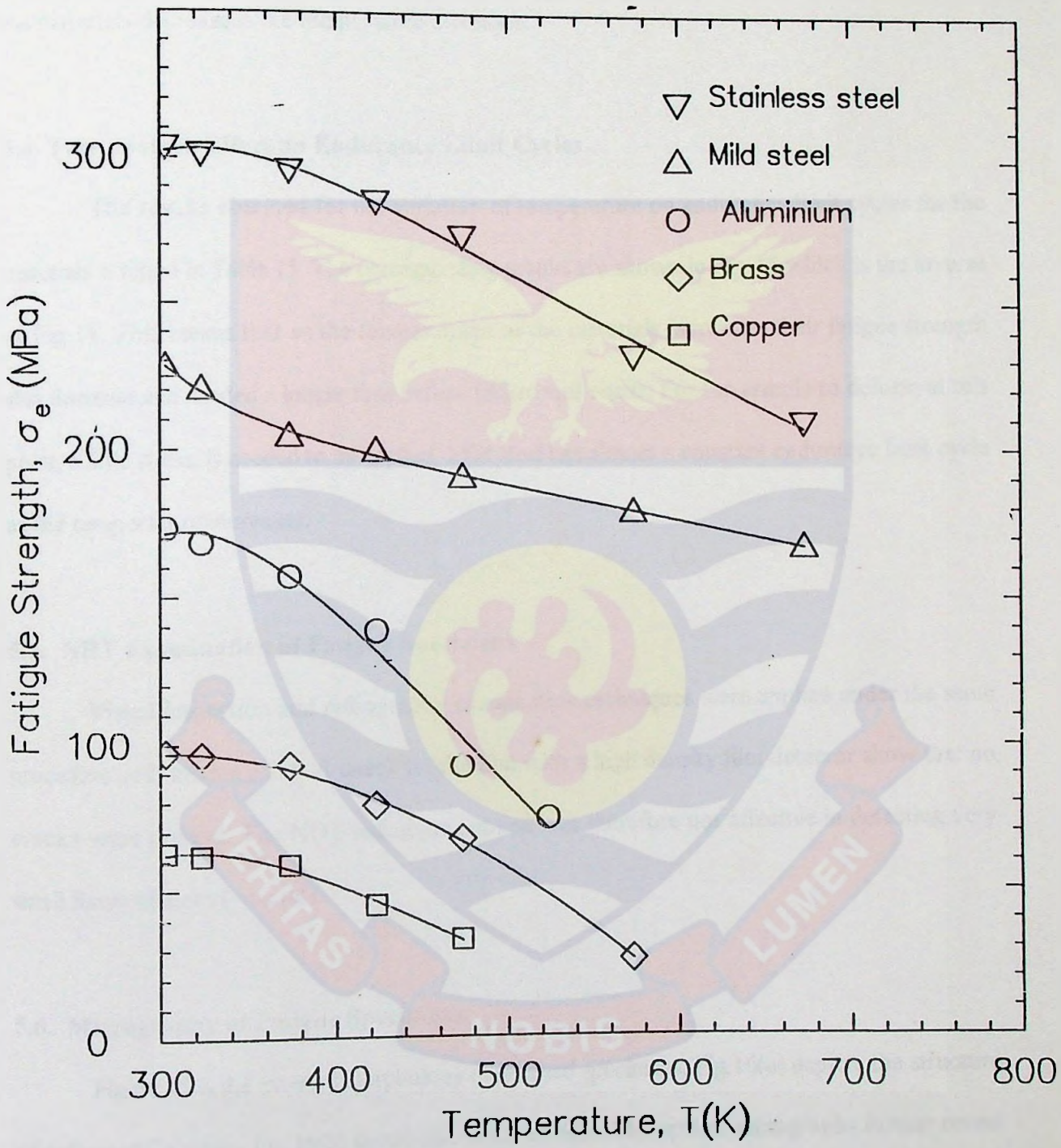

Fig. 14 Plot of Fatigue Strength, σ_e versus Temperature for FCC metals and Alloys.

deformed state. In grain boundary movement, subgrain formation may occur in addition to grain growth [29]. Despite substructural changes, Table 15 clearly shows that the fatigue strength of the materials decreaseas the temperature increases.

5.4 Temperature Effect on Endurance Limit Cycles

The results obtained for the variation of temperature on endurance limit cycles for the materials si found in Table 15. The corresponding graphs are shown in Fig. 15 which is the inverse of Fig. 14. This means that as the temperatures of the materials increases, their fatigue strength also decrease and needed a longer time before failure will occur. For the sample to deform at this point, a little stress, is needed to be applied. Mild steel has almost a constant endurance limit cycle as the temperature increases.

5.5. NDT Examination of Fatigue Specimens

Visual inspection and radiography examination techniques were applied under the same procedure as in section 3.2.4. A check on the film with a high density film detector show that no cracks were present. The NDT technique applied was therefore not effective in detecting very small flaws of sizes (~1 μm^2).

5.6. Micrography of Fatigue Specimens

Figure. 15 is the external morphology of fatigued specimens. Fig. 16(a) depicts the structure of deformed Cu whiles Fig. 16(b) shows that of Cu-30%Zn. The optical micrographs further reveal the formation of fracture at the grain boundaries. Slip and twining are plastic deformation process that are strongly involved in fatigue failure mechanism [30] .In most metals at temperatures close to room temperature, slip seems to be the predominant factor in fatigue. In polycrystalline metals

Table 15 : Effect of Temperature on Fatigue Life of Specimens.

Temperature (K)	Fatigue life				
	Al, n x 10^6	Cu, n x 10^6	Cu-30%Zn, n x 10^6	Mild steel, n x 10^5	Stainless steel, n x 10^7
303	10	9.6	8	100	2
323	10.3	9.7	8.2	102	2.01
373	11	10.3	8.4	111.5	2.06
423	11.3	13.5	9.8	114.4	2.13
473	18.7	18.2	11.5	120.1	2.26
573	23.3	-	29.8	128.7	2.66
623	-	-	-	-	2.99

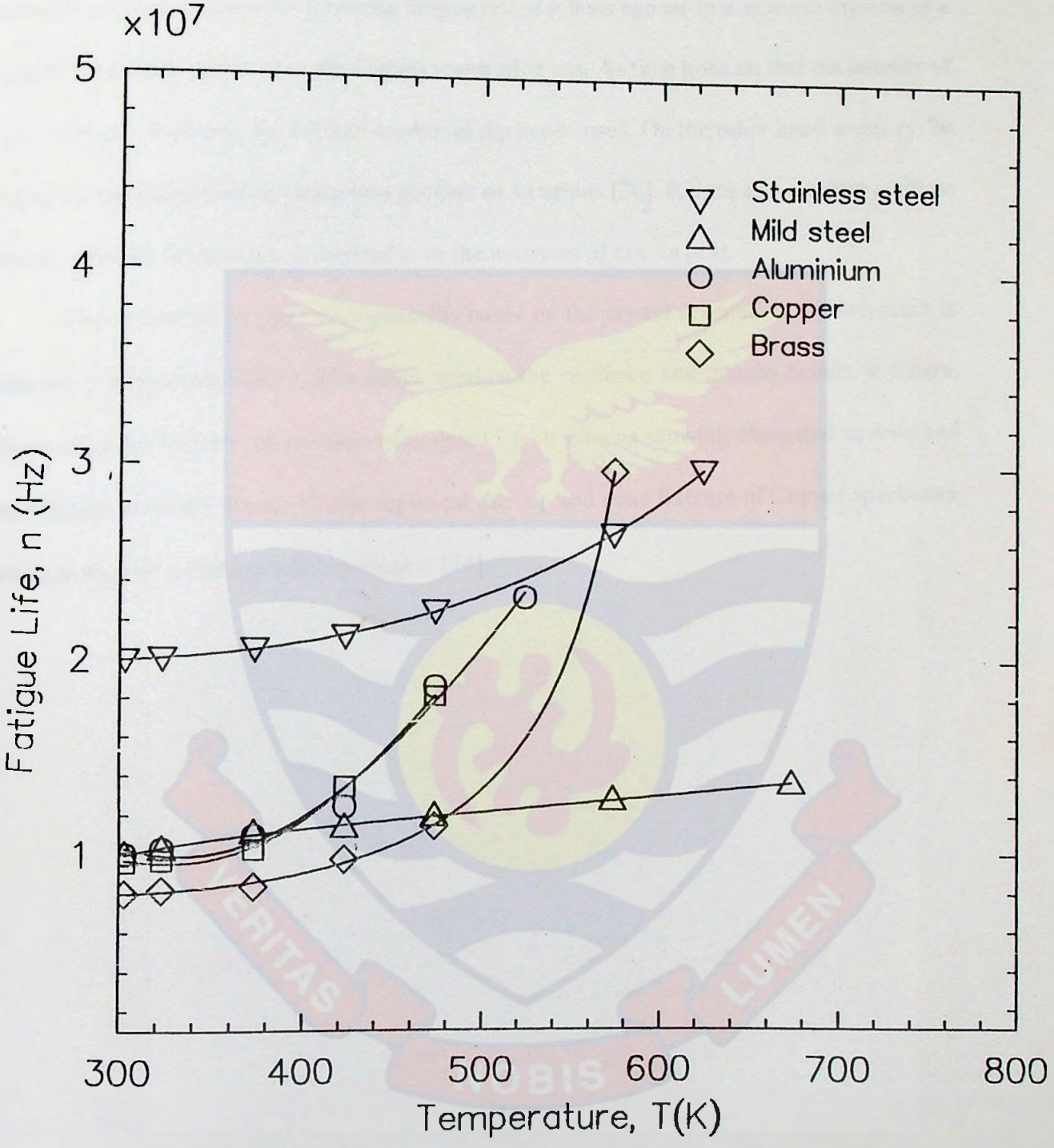

Fig. 15 Plot of Endurance Limit Cycles, n of FCC Metals and Alloys versus Temperature.

slip bands (groups of closely spaced and overlapping slip lines) are observed to form on specimens prior to fracture [29]. During fatigue test slip lines appear first in those crystals of a specimen whose slip planes have the highest resolved stress. As time goes on and the number of stress cycles too increases, the size and number of slip bands rises. On the other hand under cyclic loading the slip bands tend to group into packets or striations [30]. Ridges and crevices are then formed, with the latter being associated with the initiation of cracks [29].

The formation of crevices is generally based on the crystal orientation. Once a crack is initiated, it progresses into cavities which weaken the specimen and thereby results in failure. Figure. 17 is the internal morphology of fatigued Cu specimens showing elongated cavities and interlinkages of cracks. Figure. 18 also represent the cup and cone fracture of Copper specimens, which is similar to that reported by Rogers [34].

(a) Cu

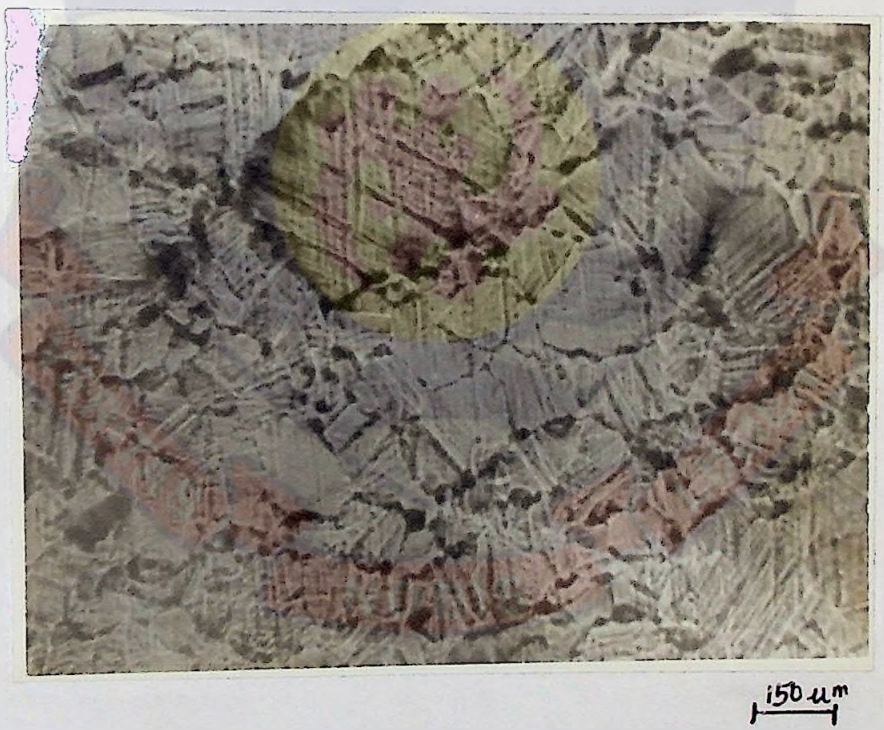

(b) Cu-30%Zn

Fig.16. External Morphology of fatigued specimens (a) Cu, (b) Cu-30Zn

(a) Etched

(b) Unetched

Fig. 17: Internal Morphology of fatigued Cu specimens (a) etched, (b) unetched, showing elongated cavities and interlinkages of cracks.

(a) 0.64X

(b)

Fig.18. : (a) Fractured Cu specimen (b) Cup and Cone fracture of Cu specimens

CHAPTER SIX

MODELLING OF FATIGUE CRACK GROWTH AND FRACTURE

6.1. Quantitative Interpretation of Fatigue-life Data

A rotating cantilever under single point loading undergoes a series of tension and compression as shown in Fig.19(a). As the material goes through constant rotation, the state of tension and compression also alternates. The state of tension is denoted by positive sign, while a negative sign depicts compression and zero as the neutral state. By virtue of the loading, the top part of the gauge length is subjected to tension at P_1. When A moves to P_2, A is subjected to compression which is later followed by stress reversals.

A material that changes state from tension to compression decreases in length as compared to the original length, and vice- versa, a change from compression to tension causes an increase in length as shown in Fig.19(b) and Fig.19(c) respectively. The changes of state of tension and compression followed by reversals initiate cavities which become interlinked and coalesced along grain boundaries leading to (micro and macro-cracks) and resulting in failure.

Stress reversals from tension and compression causes crack opening and crack closure. From Fig.20 at A, the material is under tension and thereby causing the crack to open. At B, the material is not fully subjected to compression and as such the crack tip starts to close. At point C, compression is at its maximum state and therefore leads to the closure of the crack. Finally at D, the state changes from compression to tension and crack tip starts to open. Crack closure mechanism does not completely heal the crack and a residual crack will remain per each stress reversal leading to crack propagation and Griffith type of failure [7].

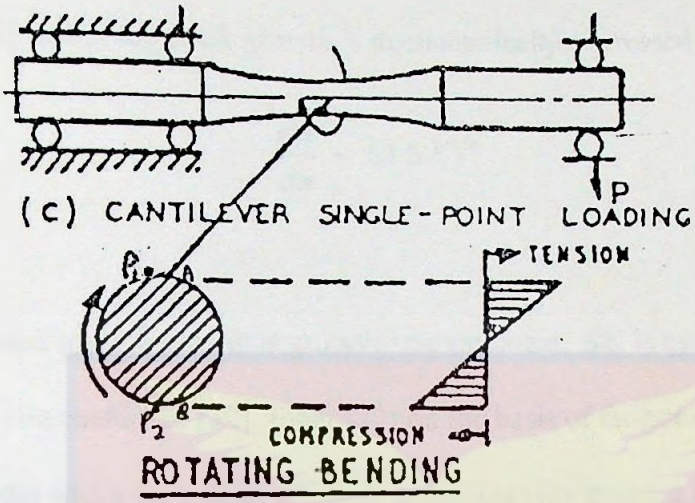

(a)

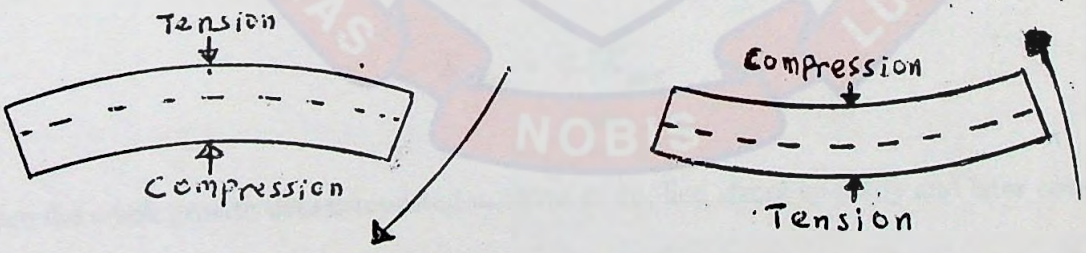

(b) (c)

Fig. 19 (a) Rotating cantilever under single point loading. Stress-reversal representation (b) Tension-Compression and (c) Compression-Tension

6.2. Model for Fatigue Crack Growth and Fracture

Paris [32] model for crack growth is mathematically expressed as

$$\frac{da}{dn} = C(\Delta K)^m \tag{6.1}$$

where da/dn is crack growth rate, m is growth rate exponent, ΔK is cyclic stress intensity and C is crack growth rate coefficient [32]. Elber [33] on the basis of fatigue crack closure experiment developed a model which include an effective stress intensity range ΔK_{eff}, which can be used to describe variable amplitude load histories . He also postulated that fatigue crack can grow only during that portion of the load cycle when crack tip is open and is being represented as [32]

$$\frac{da}{dn} = C_o(\Delta K_{eff})^m \tag{6.2}$$

where $\Delta K_{eff} = K_{max} - K_{min}$ if $K_{min} > K_{open}$

where K_{open} is the applied stress intensity required to open the crack, K_{max} is the maximum applied stress and K_{min} the minimum applied stress . For constant amplitude, and zero to maximum loading [33],

$$K_{open} = 0.3K_{max} \tag{6.3}$$

when the crack growth data is reported in terms of applied stress intensify and later converted to terms of effective stress intensity [33]

$$C_o = \frac{C}{(0.7)^m} \tag{6.4}$$

Figure 21 gives the explanation for the mechanization of fatigue crack closure. In Fig.21(a), a plastic zone is formed ahead of all cracks. As a fatigue crack grows through these zones an envelope or plastically deformed material is left in the residual compressive stress that were caused by the tensile deformations at the crack tip as shown in Fig.21(b).The residual stresses are stored internally within the structure (metal) during deformation as a tangled network of dislocations and of about 10% of the applied stress [23]. These stresses normally increase the total energy of the structure. Residual stresses are not uniform throughout the deformed metal. These compressive residual stresses must be overcome by external tensile loads before the crack up can open so that plastic strains and hence, crack growth can occur [23,33].

The applied load is related to the stress intensity as follows

$$K = \sigma \sqrt{(\pi a)}\, f(\frac{a}{w}) \qquad (6.5)$$

where σ is applied stress, a is crack length, w is specimen width and f(a/w) is a geometric factor.

By using Paris law and with no experimental work done on unnotched specimens, modelling of fatigue crack was done for Stainless steel and Aluminium. Using the data provided by materials characterization [31] i.e. m = 3, C = 7.5 x 10^{-7} mm/cycle for Stainless steel and m = 3, C = 2.5 x 10^{-7} mm/cycle for Aluminium. ΔK values were determined for Stainless steel and Aluminium respectively. Modelling was based on crack growth rate (da/dn) values ranging from 10^{-8} - 10^{-1} mm/ cycle and the results are shown in Table 16 and Fig.22.

The plot for the model was linear for both Stainless steel and Aluminium. This shows that for these materials, Paris law is obeyed between crack growth rate of 10^{-7} - 10^{-2} mm/cycle and hence the longer period before fracture occurred.

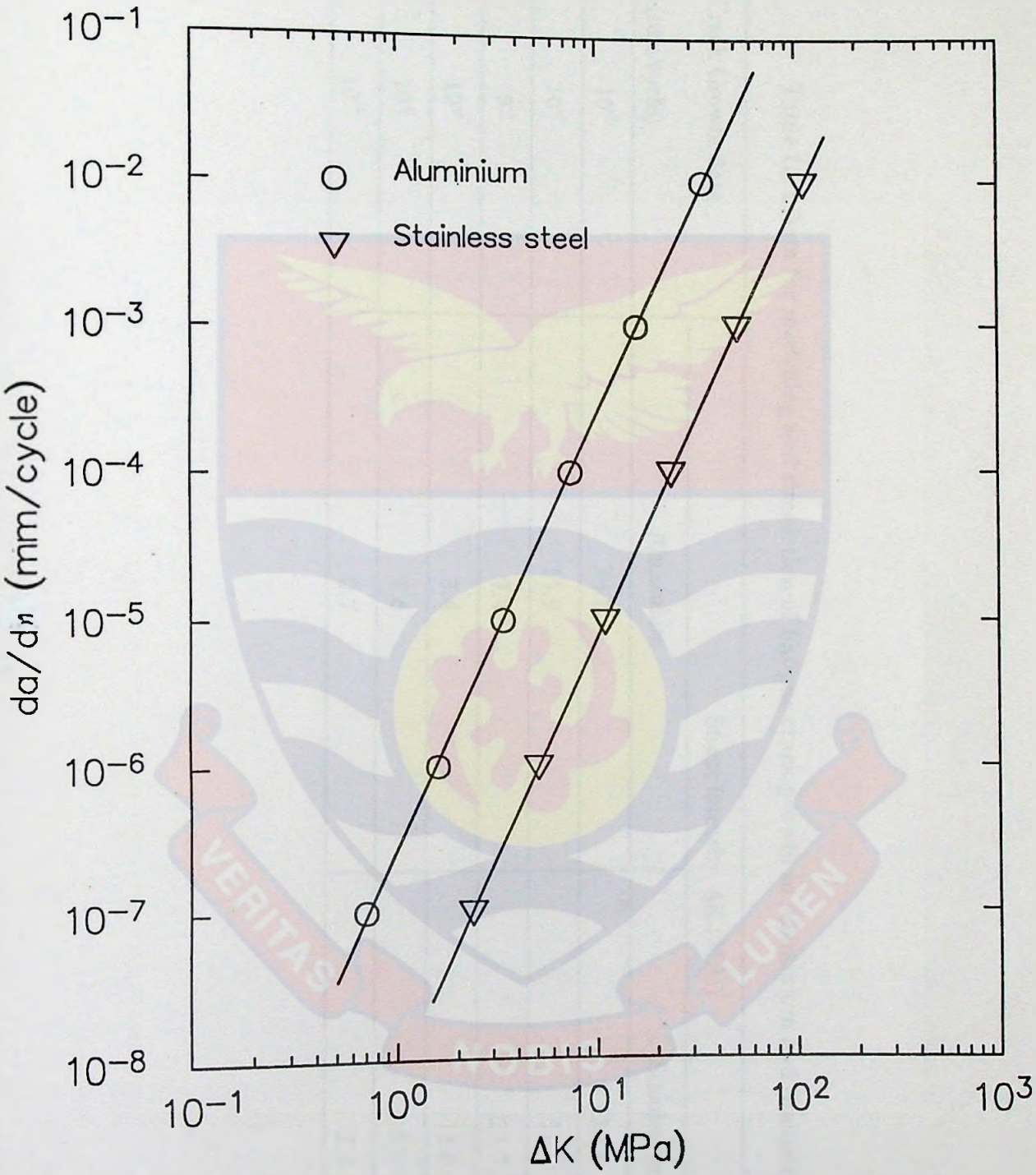

Fig.22. Plot of Crack Growth Rate against Stress Intensity factor for Aluminium and Stainless steel.

Table 16. : Data for modelling and simulation of Fatigue crack growth in Aluminium and Stainless steel.

Fatigue Crack Growth Rate (da/dn) (mm/cycle)	Stress Intensity ΔK (MPa)	
	Aluminium	Stainless steel
10^{-2}	34.2	110.1
10^{-3}	15.9	51.1
10^{-4}	7.4	23.7
10^{-5}	3.4	11.0
10^{-6}	1.6	5.1
10^{-7}	0.7	2.4

CHAPTER SEVEN

DISCUSSION AND CONCLUSIONS

7.1. Discussion

The purpose of this investigation on fatigue damage assessment of FCC metals and alloys is to study the cycle deformation and fatigue fracture of these materials in an attempt to determine the fatigue life. The results obtained would serve as a criteria to be used to advise local establishment and small factories that use large amounts of these materials in their production.

It was observed that fatigue deformation by rotating bending result from residual stresses which cause crack opening, extension and propagation. For example high compressive residual stresses may be present at the surface of a rolled plate and high tensile stresses may be stored in the center. If a small amount of metal from one surface of a cold-work is machined, metal that contains only compressive stresses will be removed. In order to restore the balance, the plate must distort leading to bending [23]. Sometimes components that are subjected to fatigue failure can be strengthened by shot peening. Bombarding the surface with steel shot propelled at a high velocity introduces compressive residual stresses at the surface; the compressive stresses significantly increase the resistance of the metal surface to fatigue failure [23].

The endurance limit, σ, obtained for the materials at room temperature ranges between 62.0 - 340.0 MPa. Investigation of fatigue strength dependance on temperature shows a decrease in fatigue strength of the materials with temperature increase. This happens as a result of diffusion of atoms into lattice vacancies after being thermally activated and thereby lowers the energy of the specimens.

In general, the strength of metals increases with decrease in grain size. This effect of grain size has been found in many cases to follow the well known Hall Petch relation [35, 36]

$$\sigma = \sigma_i + Kd^{-0.5} \quad (7.1)$$

where σ is the tensile yield or flow stress, d the grain size, and σ_i and K material constants. Two explanations proposed for the effect of grain size on the flow stress of metals are the dislocation pile up model of Hall and Petch [35,36] and work hardening model of Conrad [37, 38]. These are illustrated in Fig.23 and Fig.24 respectively. In the pile-up model shown in Fig.23 the effect of grain size is on the number of dislocations, pile up in the length δ between a source within the grain and grain boundary, and in turn on the stress concentration at the head of the pile-up, which causes multiplication or motion of dislocations at position A immediately ahead of the pile-up or at B a distance l ahead of the pile-up.

In the work-hardening model as shown in Fig.24 it is assumed that, for a given strain, a higher density of dislocations occurs in a fine-grain specimen than in one of a coarser grain size. This higher density leads to a higher average internal stress and therefore to a higher flow stress. The effect of grain size on the flow stress in this model is thus an indirect effect through its influence on the density of dislocations. Moreover, the model emphasizes the motion of dislocation throughout the grain, rather than the behaviour in the immediate vicinity of the grain boundary.

A plot of endurance limit σ_e and grain size d, for the FCC metals and alloys as shown in Fig.24 shows that endurance limit σ_e decreases with increase in grain size, which is a confirmation of Hall-Petch relation [35, 36].

Frost [39] also suggested that at the endurance limit the change over depth or critical crack l_c is of the order of the grain size. Consequently if $(\Delta\sigma^3 l_c)$ critical is a material constant,

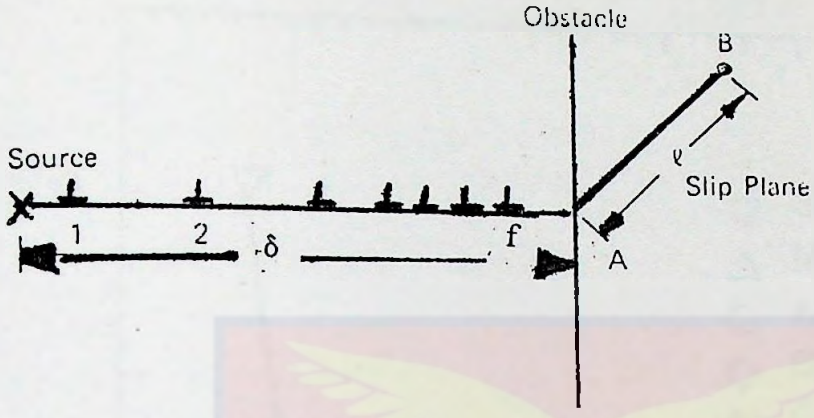

Fig.23 Schematic diagram of the pile-up model (f is the number of dislocation pile up in the length δ between the grain and grain boundary)

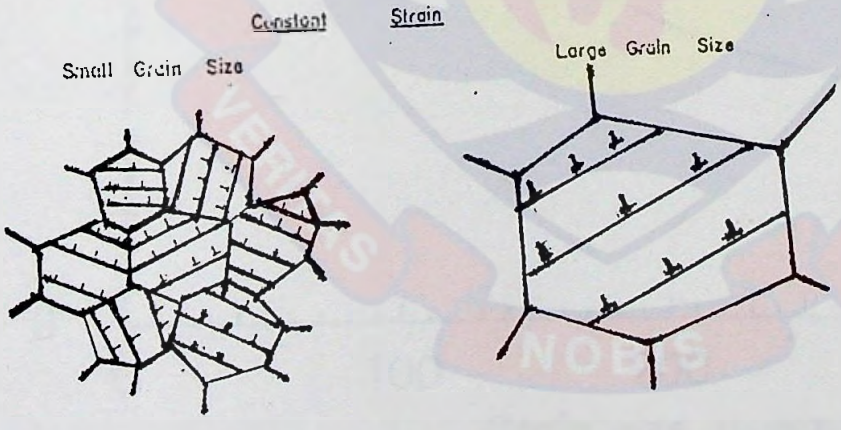

Fig.24 Schematic diagram of the pile-up model for the effect of grain size on the flow stress of metals

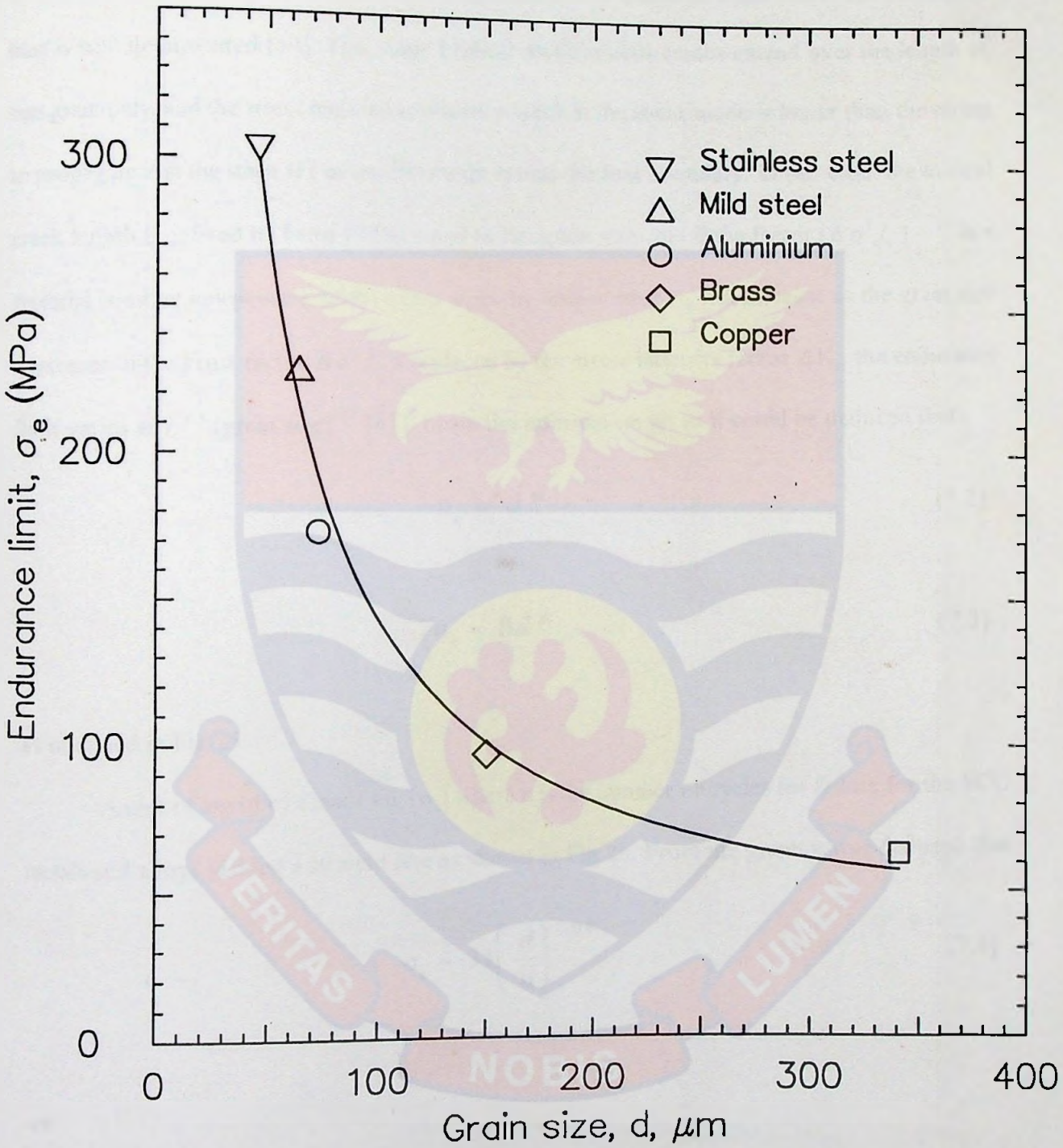

Fig.25. Plot of Endurance limit, σ_e versus Grain size, d

decreasing the grain size will result in an increase of the fatigue limit.

The formation of surface slip band micro cracks or fissures at stress below the endurance limit is well documented [40]. This stage I (shear mode) micro-cracks extend over the length of one grain only, and the stress required to initiate a crack in the shear mode is lower than the stress to propagate it in the stage II (or tensile) mode across the first boundary. In this case, the critical crack length l_c defined by Frost [39]is equal to the grain size, and if the factor $(\Delta\sigma^3_c l_c) = C$ is a material constant independent of the grain sizes the fatigue limit σ_c will increase as the grain size decreases. If the Frost factor $\Delta\sigma^3_c l_c$ is replaced by the stress intensity factor ΔK_c, the endurance limit varies as $l_c^{-0.5}$ (grain size)$^{-0.5}$ [41]. From the information given it could be deduced that

$$\sigma_c \propto d^m \tag{7.2}$$

$$\sigma_c = \beta d^m \tag{7.3}$$

as obtained in Fig.25.

A plot of log (d/n) against log (σ_c) where n is the number of cycles for failure for the FCC metals and alloys yielded a straight line as shown in Fig.26. From the graph it was deduced that

$$\sigma_c = 31\left(\frac{d}{n}\right)^{-0.6} \tag{7.4}$$

or

$$\sigma_c \propto d^{-0.6} \tag{7.5}$$

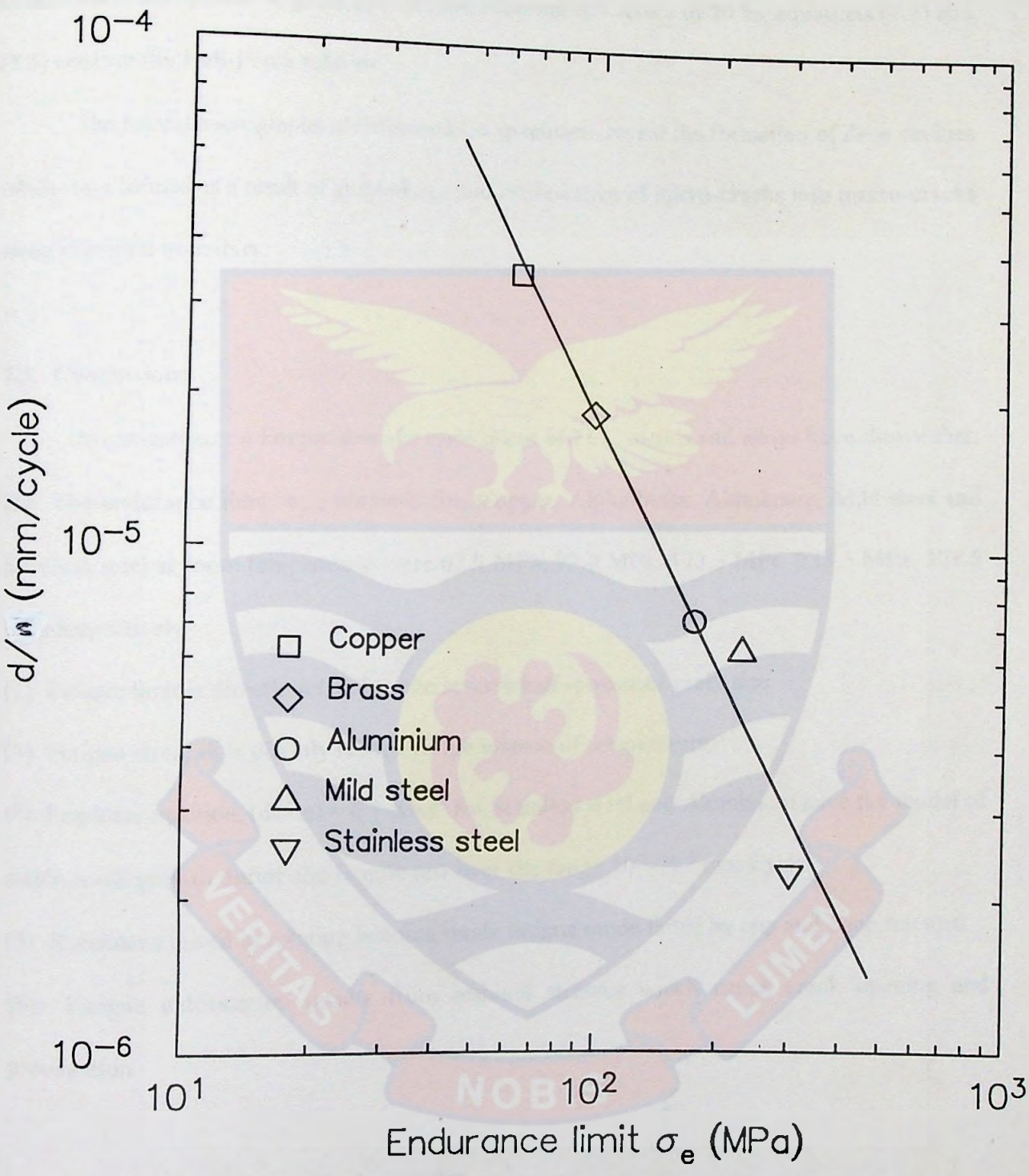

Fig.26.Plot of Grain size per cycle (d/n) versus endurance σ_e limit of FCC metals and alloys

which is an equivalent of the Hall-Petch equation for fatigue. Hence fatigue limit is directly related to the inverse half-power of grain size. Within experimental errors of 20 %, equations (7.4) and (7.5) confirm the Hall-Petch relation.

The optical micrographs of deformed Cu specimens reveal the formation of deep cavities which were formed as a result of interlinkage and coalescence of micro-cracks into macro-cracks along the grain boundary.

7.2. Conclusions

Investigations on fatigue damage assessment of FCC metals and alloys have shown that:

(1) The endurance limit, σ_e, obtained for, Copper, Alpha-brass, Aluminium, Mild steel and Stainless steel at room temperature were 62.9 MPa, 97.0 MPa, 173.3 MPa, 228.1 MPa, 303.5 MPa respectively

(2) Fatigue limit is directly related to the inverse half-power of grain size.

(3) Fatigue strength is directly related to the inverse of temperature.

(4) Empirical equation, $(da/dn) = C(\Delta K)^m$ for Stainless steel and Aluminium gave the model of stable crack growth during the fatigue test over the range 10^{-7}-10^{-2} mm/Cycle.

(5) Specimens tested in rotating bending mode fatigue mode failed by cup and cone fracture.

(6) Fatigue deformation results from residual stresses which cause crack opening and propagation.

7.3. Application of Fatigue in Industries

The phenomenon of fatigue is mostly applied in the metal industry. For instance, steel is normally used to manufacture axles of cars in the automobile industry where the axle undergoes a cyclic load during service. To enhance the service life of the axle, the stress should be below the

fatigue strength in order to prevent failure.

Kabel metal for instance makes use of aluminium and copper in the production of electrical cables. To get the final diameter of the wire, the material is subjected to cyclic load through dicing.For longer service life and prevention of failure, the final stress should be below the fatigue strength.

In the production of aluminium cooking pans, the finished product is achieved by the use of moulds in the production line. The mould through cyclic load brings out the finished product. Deformation normally takes place when the applied stress is greater than the fatigue strength hence the product does not last long when in service. It is therefore advisable for firms like the Pioneer Aluminium Company to apply stresses which are below the fatigue strength of aluminium in their production line and thereby prevent failure during use.

7.4. Suggestion for Further Research

Cavitation studies should be undertaken using image processing facilities to investigate the internal microstructure of deformed specimens of the FCC metals and alloys to obtain detailed information on cavity statistics, orientation, roundness coefficient, area and perimeter.

Furthermore, scanning and transmission electron microscopy of the deformed specimen should be undertaken to supplement data on deformation substructures including dislocation configurations.

REFERENCES

[1]. International Conference for Standardization, General Principles for Fatigue Testing of Metals, Geneva. 1964.

[2]. Whöler, A., "Versuche iiber die Festigkeit der Eisenbabwagnachen", *Zeitschrït fiir Bauwesen, Lo*,1860. English Summary 1867, *Engineering*,4, pp. 160 - 161.

[3] Ewing, J.A. and Humfrey, J.C. "The Fracture of Metals under Rapid Alternations of Stress", *Philosophical Transactions of the Royal Society*, London, A 200, 1903, pp. 241 - 250.

[4]. Coffin, L.F.," A Study of the Effect of Cyclic Thermal Stress on a Ductile Metal", *Transactions of the American Society of Mechanical Engineers*, 76, 1954, pp. 931 - 950.

[5]. Manson, S.S., Behaviour of Materials under Conditions of Thermal Stress: National Advisory Commission on Aeronautics Report, 170, Clevaland: Lewis Flight Propulsion Laboratory, 1954.

[6]. Inglis C.E., "Stresses in a Plate due to the Presence of Cracks and Sharp Corners", *Transactions of the Institute of Naval Architecture*, 55, 1913, pp. 219 - 241.

[7]. Griffith, A. A., "The Phenomenon of Rupture and Flaw in Solids", *Philosophical Transactions of the Royal Society London*, A221, 1921, pp. 163 - 197.

[8]. Irwin, G.R., "Analysis of Stress and Strains near the end of a Crack Traverssing a Plate", *Journal of Applied Mechanics*, 24, 1957, pp. 361 - 365.

[9]. Paris, P.C., Gomez M.P., and Anderson, W.P., "A Rational Analytic Theory of Fatigue", The Trend in Engineering, 13, 1961, pp. 9 - 14.

[10]. Suresh, S., Fatigue of Material, Mechanism, Total-life and Fabrication: Cambridge University, U.K, 1996.

[11]. Ayensu, A. and Longdon, T.G.," The Inter-Relationships between Grain Boundary Sliding

and Cavitation during Creep of Poly crystalline Copper" *Metallurgical and Materials Transactions* Vol. 27A, 1996, pp. 901 - 907.

[12]. Man, J.Y., Fatigue of Materials: Melbourne University Press, Carlton, Australia, 1967 First Edition.

[13]. Bolton, W., Newness Engineering Materials Pocket Book: Heineman Publishers Ltd. Oxford, 1989, First Edition.

[14]. Rollason, E.C. Metallurgy for Engineers: Edward Arnold Publishers Ltd., Norwick, 1978, Fourth Edition.

[15]. Cottrel, A., An Introduction to Metallurgy: Edward Arnold Publishers Ltd., Norwick 1978, Fourth Edition.

[16]. Snowden, K.U., Strathers P.A. and Hughes D.S., "Grain-boundary Migration in Metals Fatigued at High Temperatures", *Nature*, Vol. 261, 1976, pp. 305 - 306.

[17]. Thewlis J., Encyclopaedic Dictionary of Physics: Pergamon Press, Oxford, 1961, Vol. 1 - 2.

[18]. Lakhtin, Y., Engineering Physical Metallurgy: Foreign Languages Publishing House, Moscow, 1960.

[19]. Vastava, R.B., PhD Thesis: University of Southern California, Los Angeles, 1978.

[20]. Danso, K.A., Exposure Chart: GAEC, Kwabenya, 1996.

[21]. Pherigo, L.G., Radiography Method: American Society for Non-destructive Testing, USA, 1930.

[22]. American Society of Mechanical Engineers, Boiler and Pressure Vessel Code: Article 2, Section V, 1992 edition.

[23]. Askeland, D.R., The Science and Engineering of Materials: University Missouri, Rolla, P.W.S Publishers, 1985, Alternate edition.

[24]. Timoshenko, S.P. and Young D.H., Elements of Strength of Materials: Van Nostrand Publishers Ltd., Canada, 1968., Fifth Edition.

[25]. Laubnitz, M.J., *Can Journal of Physics*, Vol 37, 1959, pp. 1114 - 1116.

[26]. Quainoo, G.K., M.Sc Thesis: University of Cape Coast, Cape Coast, 1992.

[27]. Morley, A., Strength of Materials: William Clowes and Sons Publishers Ltd, London, 1952, Tenth Edition.

[28]. Heywood, R.B., Design Against Fatigue: Chapman and Hall Ltd, London, 1962, First edition.

[29]. Reed-Hill, R.E., Physical Metallurgy Principles: Van Nostrand Company Ltd, New York, USA, 1973.

[30]. Forsyth, P.J.E. The Physical Basis of Metal Fatigue: American Elsevier Pub Co., Inc., New York, 1969, pp. 36 - 39.

[31]. Rogers, H.C., *Acta Met.*, 7, 750 - 752, 1959.

[32]. Paris, P.C.," The Fracture Mechanics Approach to Fatigue", *Proceeding, 10th Sagamore Conference*, Syracuse University Press.

[33]. Elber, W., The Significance of Fatigue Crack Closure: ASTM, STP, 486, 230-242 1971.

[34]. Vanderveort, G.F., "Fatigue Crack Growth Principles", *Materials Characterization* Vol.33, No.3, pp. 32 - 58, 1994.

[35]. Hall, E. O., "Deformation and Ageing of Mild steel: Discussion of Results" *Physical Society of London Proceedings*, 64, 1951, 741-753.

[36]. Petch, N.J., C. "The Cleavages Strength of Polycrystals" *Iron and Steel Institute Journal*, London, 174, 1953, 25-28.

[37]. Conrad, H.," Electron. Microscopy and Strength of Crystals", *Interscience*, 1961, 299 -

302.

[38]. Conrad, H., "Effects of Grain-size on the Lower Yield and Flow Stress of Iron and Steel", *Acta Met.*, 11, 1963, 75-77.

[39]. Frost, N.E., "The Growth of Fatigue Cracks", *Proc. First International Conference on Fracture*, Sendai, Japan, 1965.

[40]. Forest, P.G and Tate, A.E.L., "The Influence of Grain size on the Fatigue Behaviour of 70/30 Brass ", *J. Inst. Met.*, 93, 1964 - 65, 438.

[41]. Burke, J.J., and Weiss V., "Ultra fine-Grain Metals" *Proceedings of the 16th Sagamore Army Materials Research Conference*, New York, USA, 1969.